Available online at www.sciencedirect.com
ScienceDirect
Geochimica et Cosmochimica Acta 75 (2011) 3135–3154
Geochimica et Cosmochimica Acta
www.elsevier.com/locate/gca

Stabilization of extracellular polymeric substances (*Bacillus subtilis*) by adsorption to and coprecipitation with Al forms

Robert Mikutta [a,*], Ulrich Zang [b], Jon Chorover [c], Ludwig Haumaier [b], Karsten Kalbitz [d]

[a] *Institute of Soil Science, Leibniz University Hannover, Germany*
[b] *Department of Soil Ecology, Bayreuth Center of Ecology and Environmental Research (BayCEER), University of Bayreuth, Germany*
[c] *Department of Soil, Water and Environmental Science, University of Arizona, USA*
[d] *Earth Surface Science, Institute for Biodiversity and Ecosystem Dynamics, University of Amsterdam, The Netherlands*

Received 1 July 2010; accepted in revised form 3 March 2011; available online 6 March 2011

Abstract

Extracellular polymeric substances (EPS) are continuously produced by bacteria during their growth and metabolism. In soils, EPS are bound to cell surfaces, associated with biofilms, or released into solution where they can react with other solutes and soil particle surfaces. If such reaction results in a decrease in EPS bioaccessibility, it may contribute to stabilization of microbial-derived organic carbon (OC) in soil. Here we examined: (i) the chemical fractionation of EPS produced by a common Gram positive soil bacterial strain (*Bacillus subtilis*) during reaction with dissolved and colloidal Al species and (ii) the resulting stabilization against desorption and microbial decay by the respective coprecipitation (with dissolved Al) and adsorption (with $Al(OH)_{3(am)}$) processes. Coprecipitates and adsorption complexes obtained following EPS–Al reaction as a function of pH and ionic strength were characterized by Fourier transform infrared spectroscopy (FTIR) and X-ray photoelectron spectroscopy (XPS). The stability of adsorbed and coprecipitated EPS against biodegradation was assessed by mineralization experiments for 1100 h. Up to 60% of the initial 100 mg/L EPS-C was adsorbed at the highest initial molar Al:C ratio (1.86), but this still resulted only in a moderate OC mass fraction in the solid phase (17 mg/g $Al(OH)_{3(am)}$). In contrast, while coprecipitation by Al was less efficient in removing EPS from solution (maximum values of 33% at molar Al:C ratios of 0.1–0.2), the OC mass fraction in the solid product was substantially larger than that in adsorption complexes. Organic P compounds were preferentially bound during both adsorption and coprecipitation. Data are consistent with strong ligand exchange of EPS phosphoryl groups during adsorption to $Al(OH)_{3(am)}$, whereas for coprecipitation weaker sorption mechanisms are also involved. X-ray photoelectron analyses indicate an intimate mixing of EPS with Al in the coprecipitates, which is not observed in the case of EPS adsorption complexes. The incubation experiments showed that both processes result in overall stabilization of EPS against microbial decay. Stabilization of adsorbed or coprecipitated EPS increased with increasing molar Al:C ratio and biodegradation was correlated with EPS desorption, implying that detachment of EPS from surface sites is a prerequisite for microbial utilization. Results indicate that the mechanisms transferring EPS into Al–organic associations may significantly affect the composition and stability of biomolecular C, N and P in soils. The observed efficient stabilization of EPS might explain the strong microbial character of organic matter in subsoils.

1. INTRODUCTION

Microorganisms play a central role in fundamental cycles of many elements including carbon, nitrogen,

* Corresponding author. Tel.: +49 511 762 2622.
E-mail address: mikutta@ifbk.uni-hannover.de (R. Mikutta).

0016-7037/$ - see front matter © 2011 Elsevier Ltd. All rights reserved.
doi:10.1016/j.gca.2011.03.006

phosphorus, and sulfur. Biofilms, cell lysis, and exudation products are important sources of microbial-derived compounds in soils (Beveridge et al., 1997). Extracellular polymeric substances (EPS) comprising a mixture of polysaccharides, amino sugars, proteins, teichoic, and nucleic acids (Kumar et al., 2007) are continuously produced during growth and metabolism of the soil heterotrophic biomass. Bacterial EPS fulfill important functions in soil environments, such as attaching bacteria to mineral surfaces, protecting them from dehydration, or capturing nutrients. Fate of this EPS is diverse; some are sorbed to bacterial cell walls or retained within biofilms and other portions are actively exuded into the soil solution (Omoike and Chorover, 2004; Leone et al., 2006). Once released into soil, EPS are subjected to potential aggregation with polyvalent metals or sorption to mineral surfaces, thus leading to the enrichment of microbial-derived carbohydrates and proteins in the clay (<2 μm) fraction or in high-density mineral–organic associations (Davis, 1982; Beveridge et al., 1997; Marschner et al., 2008; Mikutta et al., 2009). EPS-derived substances can therefore constitute a significant mass fraction of stabilized organic matter (OM) in soils.

Since polyelectrolytic EPS contain various ionizable functionalities such as carboxyl, phosphoryl, amino, and hydroxyl groups (Omoike and Chorover, 2004; Badireddy et al., 2008), they can modify the charge and hydrophilicity of mineral surfaces, thereby conditioning surfaces for bacterial attachment, colonization, and biofilm formation. In soil, bacterial exudates may participate in many ecologically relevant processes. For example, EPS can sorb or flocculate other OM constituents (Esparza-Soto and Westerhoff, 2003; Ding et al., 2008), bind toxic metals (Guibaud et al., 2006; Kumar et al., 2007; Aguilera et al., 2008; Kiran and Kaushik, 2008), promote the dissolution of minerals (Zhu et al., 2008), and enhance aggregate stability (Watanabe et al., 1999; Jaisi et al., 2007). Moreover, as EPS comprise intrinsically labile compounds, they provide a readily available C source for biosynthesis (de Brouwer et al., 2002) although an unknown portion may escape microbial utilization via sorption to mineral surfaces or complexation with metals.

Omoike and Chorover (2006) and Omoike et al. (2004) studied the adsorption of EPS isolated from *Bacillus subtilis* to goethite (α-FeOOH), a common crystalline Fe oxide in soil. Sorption was shown to be dominated by ligand exchange reactions between surficial Fe–OH groups and P-containing functionalities of EPS. Importantly, a selective uptake of P- and N-rich compounds was observed, demonstrating that the composition of aqueous-phase EPS is significantly altered because of the preferential adsorption of particular EPS fractions (Omoike and Chorover, 2006). Consequently, in order to understand the behavior and properties of EPS in natural soil environments, it is crucial to examine sorption processes and their effects on the EPS composition and properties. The composition of sorbed EPS is also dynamic because of component-selective desorption and biodegradation in open, bioactive soil systems. Assessment of sorption–desorption properties of EPS and their effects on biodegradation is thus important to appraise the potential contribution of EPS to OM stabilization.

Similar to Fe (oxyhydr)oxides, Al (hydr)oxides comprising large specific surface areas contribute significantly to the OM sorption capacity of acidic soils (Kaiser and Guggenberger, 2000). In addition, as shown by Scheel et al. (2007), stabilization of forest floor layer-derived OM in mineral–organic associations can also occur via coprecipitation with aqueous-phase Al(III), whose prevalence in oxic soil pore water typically exceeds that of Fe(III) because of the higher solubility of Al relative to Fe hydroxides. However, the extent and mechanisms of EPS adsorption to Al (hydr)oxides or complexation/coprecipitation with aqueous Al species, and the consequences of such reactions for the properties of sorbed versus aqueous-phase EPS remain unknown.

The present study addresses the influence of Al species on EPS stabilization. Specifically, by using macroscopic, spectroscopic, and incubation techniques, we examined (i) the mechanisms of EPS–Al complex formation by adsorption (using amorphous $Al(OH)_3$ as a model sorbent representing poorly-crystalline Al oxides in soil) and coprecipitation, (ii) chemical fractionation processes associated with these two processes, and (iii) the stability of adsorbed and precipitated EPS against desorption and biodegradation. In order to assess the sum effect of solid-phase interaction on bulk EPS stabilization, the stability against biodegradation was assessed for both *adsorbed* and *coprecipitated* EPS and the corresponding *non-sorbed* aqueous-phase EPS fraction.

2. MATERIALS AND METHODS

2.1. Notations and terminology

In the context of this paper, '*coprecipitation*' denotes a process wherein monomeric or polymeric aqueous Al species form a mixed Al–organic solid that evolves from solution following reaction with EPS. Depending on conditions of formation, such coprecipitates may comprise aggregated complexes of monomeric or polymeric Al with EPS, or EPS adsorbed to the surfaces of neoformed $Al(OH)_{3(am)}$. In contrast, '*adsorption*' refers to production of EPS surface excess from uptake onto surfaces of $Al(OH)_{3(am)}$ colloids that were precipitated prior to reaction with EPS. Coprecipitation and adsorption are two distinct mechanisms of EPS removal from solution that can both be included under the more general term EPS '*sorption*'. '*Fractionation*' of EPS results from the preferential adsorption or coprecipitation of specific EPS components, as reflected, e.g., in the non-stoichiometric solid-solution partitioning of EPS-C, -N, -P, and -S, as well as in preferential removal of particular biomolecular components (e.g., polysaccharides or proteins). Sorptive fractionation reactions result in the formation of '*non-sorbed*' and '*sorbed*' EPS in the aqueous and solid phase products, respectively. EPS '*mineralization*' refers to the oxidative biodegradation of EPS-C to CO_2.

2.2. Aluminum hydroxide

Amorphous $Al(OH)_3$ was precipitated by slowly neutralizing a solution of 2 M $AlCl_3$ with NaOH. The precipitate

was washed with deionized water and freeze-dried. The specific surface area (*SSA*) of the product was analyzed by N_2 adsorption at −196 °C with a Nova 2010 surface area analyzer (Quantachrome Corp., Boynton Beach, USA) after degassing the sample at 40 °C for 48 h. The Brunauer–Emmett–Teller *SSA* was 102 ± 2 m^2/g. The X-ray diffraction pattern of $Al(OH)_{3(am)}$ was recorded with a D5000 instrument (Siemens AG/Bruker AXS, Karlsruhe, Germany). The lack of diffraction signals confirmed the X-ray amorphous structure of $Al(OH)_{3(am)}$.

2.3. Bacterial cell cultivation, EPS purification and characterization

Isolation of EPS followed the procedure described in Omoike and Chorover (2006) using autoclaved glassware. Briefly, endospores of *B. subtilis* (American Type Culture Collection, ATCC 7003) were added to trypticase-soy-medium and activated aerobically for 24 h at 30 °C. The bacterial suspension was added to LB-Lennox-Media (5 g/L yeast extract, 10 g/L Trypton, 5 g/L NaCl) in flasks with air-conductive cellulose stoppers and incubated at 30 °C on a horizontal shaker (130 rpm). EPS were isolated from bacterial suspensions in the early stationary growth phase (Omoike and Chorover, 2006). The suspension was first centrifuged (15 min, 5000*g*) at 4 °C to remove bacterial cells; then the supernatant was centrifuged for another 50 min (10,000*g*) to separate EPS from other cell constituents. EPS was subsequently precipitated with cold (2 °C) ethanol at a volumetric ethanol:water ratio of 3:1; the suspension was left for 24 h at −18 °C (de Brouwer et al., 2002). For further purification, this step was repeated and the product freeze-dried.

Non-purgeable OC and total N was determined in EPS solutions using a multi N/C 2100 analyzer (Analytik Jena, Jena, Germany); S, P, Al, K, Ca, and Na were measured by inductively coupled plasma optical emission spectroscopy (Jobin Yvon, JY 70 plus, Longjumeau, France). Phosphate, SO_4^{2-}, Cl^-, NO_3^-, and NH_4^+ were measured by ion chromatography (DX 500, Dionex, Idstein, Germany). The amino acid composition of EPS were determined after hydrolysis of EPS in 6 M HCl for 12 h at 105 °C as described in Mikutta et al. (2010). The amino acids were measured as *N*-pentafluoropropionyl-amino acid isopropyl esters using a GCMS-QP 2010 instrument (Shimadzu Corp., Tokyo, Japan).

NMR spectra (^{1}H, ^{13}C, ^{31}P) of freeze-dried samples (150 mg) dissolved in 3 mL of 0.5 M NaOD solution were recorded with a 11.7 T Bruker DRX 500 NMR spectrometer (Bruker Analytische Messtechnik GmbH, Rheinstetten, Germany) at a temperature of 17 °C. The measuring conditions were for ^{13}C NMR: 10-mm sample tubes; spectrometer frequency, 125 MHz; inverse-gated decoupling; acquisition time, 0.16 s; delay time, 1.84 s; line-broadening factor, 100 Hz; for ^{1}H NMR: 5-mm sample tubes; spectrometer frequency, 500 MHz; homonuclear presaturation for solvent suppression; acquisition time, 1.16 s; delay time, 1 s; line-broadening factor, 2 Hz; and for ^{31}P NMR: spectrometer frequency, 202.5 MHz; no proton decoupling; acquisition time, 0.1 s; relaxation delay, 2 s; line-broadening factor, 20 Hz. Chemical shifts were measured relative to 85% H_3PO_4 in a 5-mm tube inserted into the 10-mm sample tube before the measurement of each sample.

2.4. Adsorption, coprecipitation and desorption experiments

An EPS-stock solution of 100 mg C/L was prepared. For adsorption experiments, different amounts of freeze-dried $Al(OH)_{3(am)}$ were weighed into 250 mL glass tubes and 100 mL of the EPS-stock solution were added, producing molar Al:C ratios ranging between 0.05 and 1.86 (1.0–35.0 mg $Al(OH)_{3(am)}$/mg EPS-C). For coprecipitation, an $AlCl_3{\cdot}6H_2O$ solution (20 g/L) was added to glass tubes and mixed with 100 mL of the EPS-stock solution, generating molar Al:C ratios of 0.01–0.2. All experiments were conducted in triplicate at 5 °C to reduce microbial utilization. After 18 h of equilibration on a horizontal shaker at 60 rpm, the solutions were filtered through 0.45-μm polycarbonate filters (HTTP 04700, Millipore, Bedford, USA). We observed no EPS sorption to the filter material. To study the effect of pH and ionic strength (*I*) on EPS adsorption and coprecipitation, different EPS solutions varying in pH (3.8 and 4.5) and *I* (1.7, 17, and 170 mM) were prepared. Target pH-values were achieved by dropwise addition of concentrated HCl, whereas *I* values were obtained by varying concentrations of analysis-grade $NaClO_4$ (VWR International). pH shifts <0.5 pH-units resulting from initial mixing of $Al(OH)_{3(am)}$ or $AlCl_3$ with EPS solutions were corrected to target values by addition of dilute HCl or NaOH. The mass of adsorbed or coprecipitated EPS-C, -N, -P, or -S was calculated by the difference between initial and final OC and N concentrations in the filtrate (before and after reaction with Al species); organic N was calculated as total N minus $[NO_3^- + NH_4^+]$–N; organic P as total P minus $[PO_4^{3-}]_T$–P, and organic S as total S minus $[SO_4^{2-}]$–S.

To quantify EPS desorption from solid phase products, 50 mL of a solution equivalent to the inorganic background electrolyte used in the incubation solution (NH_4NO_3: 0.24 mmol/L; K_2HPO_4: 0.20 mmol/L) was added to the moist adsorption complexes and coprecipitates, shaken for 24 h at 5 °C, and filtered to <0.45-μm. This step was repeated once and the total amount of desorbed OC was calculated by summation of OC released in each step.

2.5. Biodegradation experiments

Adsorption complexes and coprecipitates obtained at pH 4.5 were suspended in 60 mL of bi-distilled water and then incubated separately in 120-mL glass bottles. The complete polycarbonate filters (see Section 2.4) containing the adsorption complexes and coprecipitates were transferred to the incubation bottle. Replicated 60 mL samples of the bulk (*unreacted*) EPS and *non-sorbed* (aqueous phase, post-reaction) EPS solutions were likewise incubated. Polycarbonate filters were added to these treatments to ensure comparability with the incubation of the solid phases. To each incubation bottle, 1 mL of a nutrient solution (NH_4NO_3: 0.24 mmol/L; K_2HPO_4: 0.20 mmol/L) and 0.6 mL of an inoculum derived from the Oa horizon of a

Podzol (Mikutta et al., 2007) were added. Cell density of the inoculum was $\sim 6 \times 10^6$ mL^{-1}. Incubation of a glucose solution at pH 4.5 assured the functionality of the microbial community at high proton activity. After closing the bottles with a butyl septum, ~30 mL of ambient air were injected with a syringe in order to assure overpressure (~450 hPa) for chromatographic gas analyses. The bottles were incubated for 1100 h at 20 °C in the dark and were shaken every second day to minimize O_2 deficiency. Previous research showed that this period is long enough to cover most of the mineralizable C of natural OM (Scheel et al., 2007). The unreacted EPS solution and bi-distilled water with nutrients and inoculum added served as controls (each with polycarbonate filters). The mineralization of adsorbed and coprecipitated EPS was corrected for the CO_2 produced by the inoculum alone. Carbon dioxide release from the inoculum alone was negligible (<1000 ppm CO_2 in the headspace), suggesting that EPS production and mineralization from the inoculum was negligible. During incubation, gas samples were taken periodically. Head-space CO_2-concentrations were quantified with a gas chromatograph equipped with methanizer and flame ionization detector (SRI 8610C, Torrance, USA). The maximal CO_2 concentration in the headspace was 4.4 vol% for unreacted EPS (without any treatment) which is similar to values observed in soil. To accurately assess the amount of CO_2 derived from biodegradation, a set of equations was applied to account for physically and chemically dissolved CO_2:

$$N_g = \frac{pV_g}{RT} \quad (1)$$

$$N_p = \alpha \times N_g \frac{V_l}{V_g} \quad (2)$$

$$N_c = N_p \times 10^{-pK_{a1}+pH} \quad (3)$$

where $N_g = CO_2$ concentration in gas phase (mol), p = partial pressure in incubation bottle (Pa), V_g = gas volume (m^3), R = Constant [8.31451 J/(K mol)], T = temperature (K); N_p = physically dissolved CO_2 (mol), α = Bunsen absorption coefficient of CO_2 in water at 293 K (Bartels and Wrbitzky, 1959), and V_l = solution volume (0.0616×10^{-3} m^3); N_c = chemically dissolved CO_2 (mol), pK_{a1} = dissociation constant for H_2CO_3/HCO_3^- (6.38), pH = pH of solution phase. Since the pH during incubation could not be monitored continuously, the pH evolution was interpolated assuming that the proton concentration was related to EPS degradation kinetics according to:

$$C_t(H^+) = C_0(H^+)e^{-kt} \quad (4)$$

where $C_t(H^+)$ = proton concentration at time t (mol/L), $C_0(H^+)$ = initial proton concentration ($10^{-4.5}$ mol/L), k = degradation rate (1/h), and t = incubation time (h). The total CO_2 concentration (N_{total}) was then finally quantified as

$$N_{total} = N_g + N_p + N_c \quad (5)$$

By normalizing the total moles of CO_2 produced by EPS mineralization to the amount of C initially adsorbed or coprecipitated, the extent of degradation was calculated for every sampling point. An exponential degradation model was fitted to the data (Paul and Clark, 1996):

$$A_t = A_{max}(1 - e^{-kt}) \quad (6)$$

with A_t = fraction degraded at time t, A_{max} = fraction degraded at $t \to \infty$ (%), k = degradation rate (1/h), and t = degradation time (h). The overall stabilization of EPS upon interaction with $Al(OH)_{3(am)}$ or Al was quantified by comparing the summative extents of biodegradation of the *adsorbed* or *coprecipitated* EPS, plus that of their respective aqueous phase (i.e., non-sorbed) components, with those of the *unreacted* EPS.

2.6. X-ray photoelectron spectroscopy (XPS)

Selected samples were studied with XPS to reveal chemical differences between adsorbed and coprecipitated EPS, and also relative to unreacted EPS. XPS measurements were performed using a VG ESCALAB 220i XL spectrometer with non-monochromated Al Kα-radiation (E_{exc} = 1468.6 eV). Survey spectra (0–1000 eV) were recorded using a pass energy of 50 eV, while 10 eV was used for the detail scans in the C1s and N1s region. The takeoff angle was set at 90°. The pressure in the analysis chamber during measurement was always $<10^{-6}$ Pa. About 2 cm^2 of each sample were analyzed in order to obtain representative spectra. Under the measuring conditions, the FWHM of the $Ag3d_{5/2}$ peak was 1.49 eV at 50 eV pass energy and 1.0 eV for 10 eV pass energy. The composition of samples was quantified using Unifit Version 8.0 (Hesse et al., 2003). Peaks present in the spectra (O1s, C1s, N1s, P2p, Cl2p3, Al2p, Na2s) were referenced to the C signal at 285.0 eV, integrated and quantified using the manufacturer-based sensitivity factors. In contrast, the detail C1s scan was referenced to the N signal in the survey scan centered at 400.0 eV (amide N), and vice versa for the N1s peak.

2.7. Fourier transform infrared (FTIR) spectroscopy

Diffuse reflectance infrared Fourier transform (DRIFT) spectra were collected on the solid phase EPS–Al complexes, whereas transmission FTIR spectra were obtained on aqueous-phase EPS samples both before and after reaction (Omoike and Chorover, 2006). Spectra of the freeze-dried solid phase were collected in DRIFT mode using a SpectraTech DRIFT accessory after gently mixing 10 mg of solid with 300 mg of IR grade KBr powder. Samples were then packed into a stainless steel cup and scanned using pure KBr as background. The spectra of adsorbed EPS were obtained by difference of the respective adsorption complex minus the spectrum of pure $Al(OH)_{3(am)}$. For aqueous-phase EPS samples, several solution aliquots (100–1200 μL) were transferred and dried onto IR transmissive Ge windows, and spectra of EPS films were collected in transmission mode. For all samples, a total of 350–400 scans were collected over the spectral range of 400–4000 cm^{-1} at a resolution of 4 cm^{-1} using a Magna-IR 560 Nicolet spectrometer equipped with a CsI beam splitter, DTGS-detector, and OMNIC processing software.

2.8. Scanning electron microscopy (SEM)

Selected samples including unreacted and Al-species-reacted EPS were examined using a FEI Quanta 200 instrument at accelerating voltages of 20–30 kV.

3. RESULTS

3.1. Chemical properties of EPS

Cultivation of *B. subtilis* resulted in visually apparent flocculation and bacterial film formation. The purified EPS was composed of 340, 80 and 35 mg/g of organic carbon, nitrogen, and phosphorus, respectively (Table 1). Scanning electron micrographs of dehydrated EPS revealed aggregates with a small number of randomly distributed *B. subtilis* rods that were not removed during purification (Fig. 1A). Phase contrast microscopy and SYBR green staining of the EPS followed by fluorescence microscopy revealed $\sim 2.2 \times 10^7$ cells/mg EPS. Assuming the average dry weight of a procaryotic cell to be 2×10^{-13} g with half of that being assignable to carbon (Whitman et al., 1998), we estimate that cellular C contributed 2.2 mg/g EPS dry weight or 6.5 mg/g EPS-C (<1%).

Protein and polysaccharide constituents dominate in EPS and usually occur at similar mass concentrations for the experimental growth conditions employed here (Omoike and Chorover, 2004). The protein content of EPS was estimated based on XPS measurements (Dufrêne et al., 1997) with $(N/C)_{XPS} = 0.289$ (C_{PE}/C) where 0.289 is the average N:C ratio of hydrolyzable amino acids in EPS and C_{PE}/C represents the protein fraction. According to this calculation, 66% of EPS consisted of proteins with the remainder being mainly attributable to polysaccharides, with smaller contributions of nucleic acids, and phospholipids. Hydrolyzable amino acids accounted for only 19% of EPS mass with glutamic acid/glutamine being the most abundant amino acid followed by lysine > serine > asparagine/aspartic acid > alanine = glycine > others (not shown). NMR spectroscopy revealed the abundance of proteins, phosphorus compounds, and carbohydrates representing microbial exudates as well as cell wall components (Table 1). After harvesting, EPS was enriched in carbohydrates (+26%; ^{1}H NMR $\delta = 3$–4 ppm), organic P (+388%; ^{31}P NMR $\delta = 1$–3 ppm) and teichoic acids (at $\delta = 1.9$ ppm; Makarov et al., 2005) but depleted in aromatic (−63%; ^{1}H NMR $\delta = 5.5$–10 ppm) and carboxylated (−3%; ^{13}C NMR; $\delta = 160$–200 ppm) compounds relative to the cultivation medium. According to ^{13}C NMR, about 28% of total C can be assigned to O-alkyl C structures as occur in carbohydrates (Table 1). Beside ortho-phosphate (27%), and phosphodiesters (17%), ^{31}P NMR revealed a large percentage of phosphomonoesters (56%), which may partly represent alkaline hydrolysis products of RNA (Makarov et al., 2005) and terminal phosphate groups of phospholipids generated by EPS dissolution in NaOD for NMR spectroscopy.

3.2. Chemical fractionation during adsorption and coprecipitation of EPS

For both adsorption and coprecipitation, the amount of EPS-C removed from solution increased with initial molar Al:C ratio (Fig. 2). At comparable initial molar Al:C ratios (<0.2) more than twofold greater OC mass was coprecipitated than adsorbed (Fig. 2). Under the experimental conditions, coprecipitation resulted in a maximum of 33% OC removal (at maximum molar Al:C ratio of 0.2) whereas adsorption gave a maximum of 60% OC removal (at a molar Al:C ratio of 1.86). This corresponds to mass-based solid phase OC values of *ca.* 254 mg/g $Al(OH)_{3(am)}$-equivalent for the coprecipitate (assuming complete Al precipitation) versus 17 mg/g $Al(OH)_{3(am)}$ for the adsorption complex. Adsorption of EPS-C to $Al(OH)_{3(am)}$ did not reach capacity in this experiment as no distinct sorption plateau was observed. Surface area-normalized OC adsorption increased with decreasing initial molar Al:C ratio due to the declining availability of $Al(OH)_{3(am)}$ surface sites (Fig. 2). Similarly, the mass fraction of EPS-C in coprecipitates increased with decreasing molar Al:C ratio.

EPS-N was proportionally adsorbed relative to EPS-C, resulting in almost constant $(C:N)_{org}$ ratios of solid-bound EPS (Fig. 3). At small molar Al:C ratios, less EPS-S than EPS-C and -N was adsorbed but this difference levelled off at larger Al:C ratios (>0.80). EPS-P moieties were preferentially adsorbed to $Al(OH)_{3(am)}$ (Fig. 3). Coprecipitation of EPS by Al produced a larger variability of C, N, S, and P in the respective products. EPS-N was precipitated in similar quantity as EPS-C while EPS-P components showed again a preferential uptake at molar Al:C ratios >0.02. In

Table 1
Properties of EPS used in the study.

Solid concentration (mg/g)				Inorganic composition of EPS stock solution containing 100 mg C/L (mmol/L)								
OC	ON	$(C:N)_{org}$[a]	Amino acids	NH_4^+	NO_3^-	$H_2PO_4^-$	SO_4^{2-}	Cl^-	Mg^{2+}	Ca^{2+}	K^+	Al
340.4	88.0	3.9	186.0	0.04	<<0.01	0.18	0.02	0.90	0.01	0.03	0.11	0.004

Distribution of functional groups derived from solution–state ^{31}P, ^{13}C, and ^{1}H NMR (%)

Ortho-P	Monoester P	Diester P	Carboxyl-/carbonyl-C	Aromatic C	O-Alkyl C	Alkyl-C	Aromatic H	O-Alkyl H	Alkyl-H
>5.3 ppm	2.5–5.3 ppm	−1.0 to 2.5 ppm	160–200 ppm	110–140 ppm	60–110 ppm	0–60 ppm	5.5–10 ppm	3.0–4.8 ppm	0.1–1.8 ppm
27	56	17	17	6	28	49	1	27	39

[a] Dimensionless.

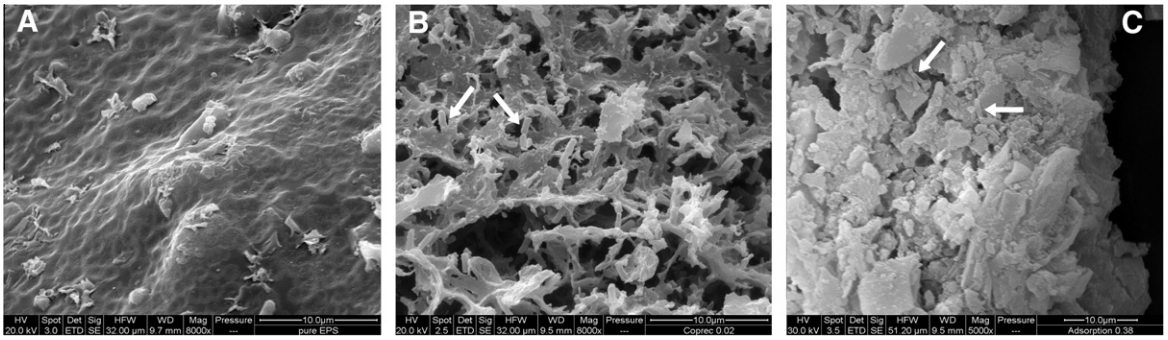

Fig. 1. Scanning electron images of (A) dehydrated isolated EPS, (B) EPS coprecipitated with Al at a molar Al:C ratio of 0.02, and (C) EPS adsorbed to $Al(OH)_{3(am)}$ at a molar Al:C ratio of 0.38. Note the rod-shaped structures of *B. subtilis* at the surfaces of the coprecipitation and adsorption complexes (white arrows).

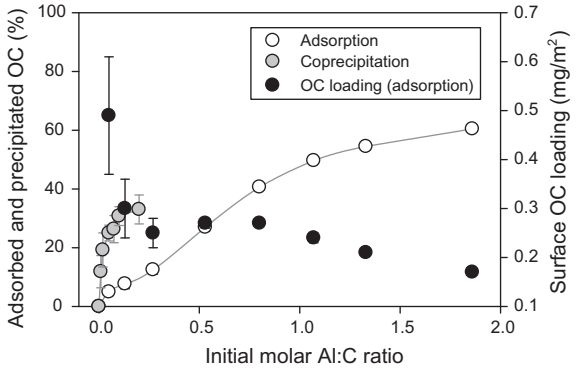

Fig. 2. Adsorption and coprecipitation of EPS as a function of the initial molar Al:C ratio. The initial EPS-C concentration and pH were 100 mg/L and 4.5, respectively. Surface OC loadings are shown for adsorption complexes only.

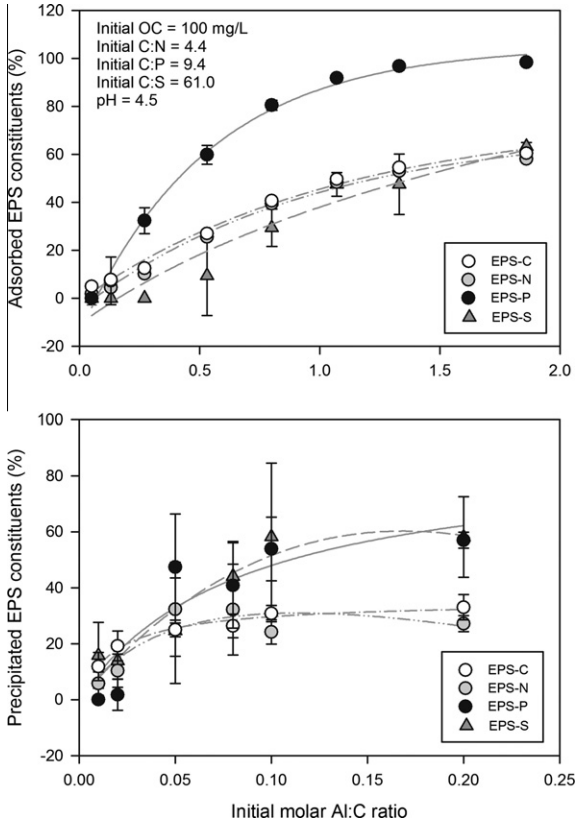

Fig. 3. Selective adsorption and coprecipitation of EPS-C, -N, -P, and -S components of EPS as a function of the initial molar Al:C ratio. The lines serve as guides only.

contrast to adsorption, EPS-S was also preferentially retained in coprecipitates at Al:C ratios >0.05.

3.3. pH and ionic strength effects

There was no statistically significant pH-dependence of EPS-C and total EPS-N adsorption to $Al(OH)_{3(am)}$ in the pH range studied (Fig. 4A). Total P adsorption declined somewhat with increasing pH. Adsorption of EPS-C as well as that of total N and total P were independent of ionic strength (I) at a molar Al:C ratio of 0.53. Coprecipitation of EPS-C was significantly greater at higher pH (4.5 versus 3.8) particularly at larger molar Al:C ratios (Fig. 4B). The same trend was observed for total N and P, respectively. Coprecipitation of EPS-C at an initial molar Al:C ratio of 0.075 significantly decreased with increasing I (Fig. 4C). Likewise, coprecipitation of total N and total P significantly declined at larger I by >37% (Fig. 4C).

3.4. Desorption of EPS

Following adsorption and coprecipitation at pH 4.5, the respective complexes were dispersed in OC-free background electrolyte. Across the complete data set (irrespective of treatment), fractional OC desorption increased with decreasing initial molar Al:C ratio (Fig. 5). The pooled desorption data follow an exponential function, suggesting only a small desorbed fraction at initial molar Al:C ratios >0.80, which translates into OC concentrations less than about 27 mg/g $Al(OH)_{3(am)}$. Within the set of coprecipitate samples, OC desorption appeared independent of the initial molar Al:C ratio. At comparable initial molar Al:C ratios (<0.2), coprecipitates released significantly more OC than did the adsorption complexes (>20% difference). Aluminum

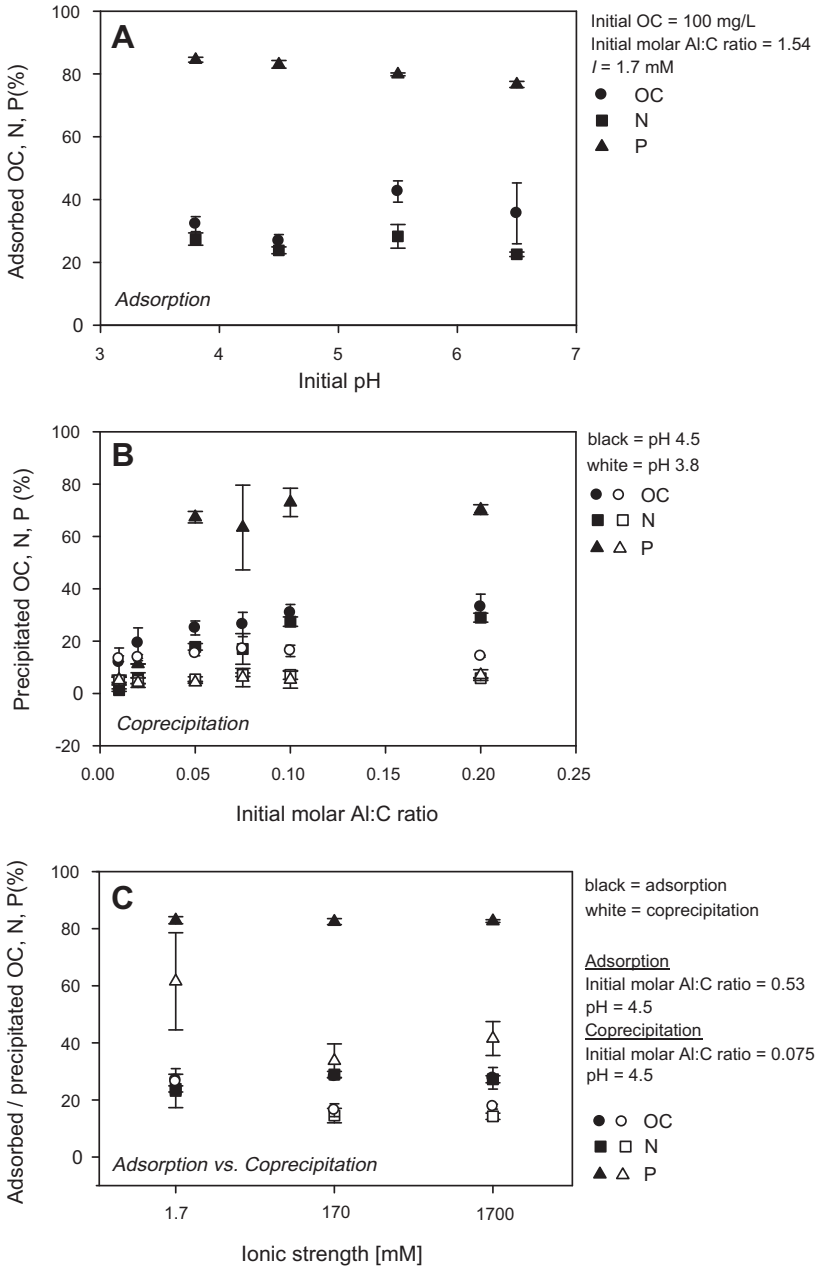

Fig. 4. pH and ionic strength (I) dependence in the adsorption and coprecipitation process of organic C, total N, and total P.

concentrations in the desorption solutions were low for the coprecipitates (<30 μM; molar Al:C ratios <0.01), suggesting that the larger fractional OC release was not caused by dispersion of Al–EPS complexes but rather fostered by the weaker bondings involved in the coprecipitation process (see Section 4.3).

3.5. Biodegradation of EPS

During the 1100 h incubation, 70 ± 2% of the EPS-C was mineralized in aqueous solution in the absence of added Al species. The overall stabilization of EPS by adsorption or coprecipitation was assessed by summing the biodegradation over the same 1100 h time period of solid-phase (*adsorption* or *coprecipitation complexes*) plus corresponding aqueous-phase (*non-sorbed*) EPS after reaction with Al species. Overall mineralization data were fit to a one-pool decay model (Table 2). In most treatments, adsorption and coprecipitation resulted in overall stabilization of EPS against microbial decay as revealed by the smaller extent of mineralization when compared to EPS alone (Fig. 6) The overall biodegradation of EPS-C (A_{1100h}) decreased with increasing initial molar Al:C ratio (Fig. 7A). Statistically significant stabilization of EPS-C was initiated at much lower molar Al:C ratio for coprecipitation (0.01) relative to adsorption (0.53). As a result,

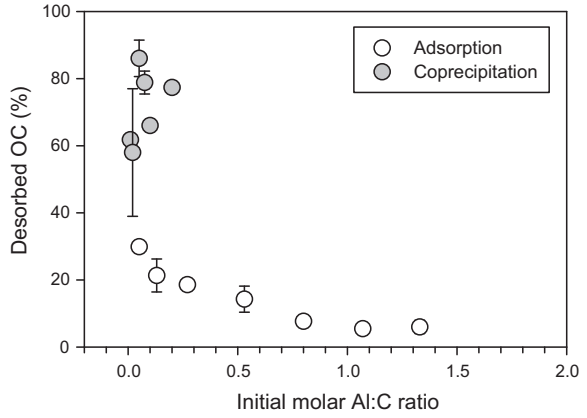

Fig. 5. Relationship between the initial molar Al:C ratio and the OC fraction mobilized in a desorption treatment at pH 4.5.

coprecipitation appeared more efficient than adsorption in stabilizing EPS-C against biodegradation at a comparable initial molar Al:C ratio of 0.2. Increasing the initial Al:C ratio in the adsorption treatment (up to 1.86) by adding more $Al(OH)_{3(am)}$ sorbent resulted in overall EPS stabilization that finally exceeded that of the precipitation products. Fig. 7B, however, illustrates that the overall biodegradation was a linear function of the solid-phase partitioning of EPS, irrespective of the mode of association (adsorption versus coprecipitation).

Fig. 8 depicts the relative contribution of solid and the solution phase EPS to overall mineralization. Mineralization of the non-sorbed EPS remained at a high level ($\geqslant$60%) in the adsorption treatments whereas that of adsorbed EPS decreased markedly to <1% with increasing molar Al:C ratio (Fig. 8). No such trends were observed for the coprecipitates. At larger initial molar Al:C ratios, mineralization values for precipitated EPS were comparable to those for non-sorbed fractions.

Table 2 shows that the one-pool degradation model when applied to the adsorption complexes alone at high initial molar Al:C ratios results in poor fits (low r^2) due to negligible mineralized EPS. A sigmoid-like relation was observed between the percentage of desorbable OC and the modeled maximal extent of biodegradation (A_{max}) for the solid-phase adsorption and coprecipitation complexes (Fig. 9). The decay rate constants, however, were not correlated with OC desorption. Conversely, a trend of faster degradation kinetics with decreasing OC desorbability was apparent for the adsorption complexes (Fig. 10), suggesting that in the case of minor mineralization of adsorbed EPS, a small portion of labile EPS was decomposed quickly.

Table 2
Mineralization results (at 1100 h) for the unreacted EPS and also for EPS products of adsorption or coprecipitation. Data include best fit parameters for the one-pool degradation model (Eq. (6)) fitted to either (i) the summed mineralization of *solid-bound* and *non-sorbed* EPS products (overall mineralization) or (ii) solid-phase EPS only (mineralization of solid bound EPS), following reaction with $Al(OH)_{3(am)}$ (adsorption) or $Al_{(aq)}$ (coprecipitation).

	Initial molar Al:C	A (%)	SE	A_{max} (%)	SE	k (1/h)	SE	r^2
Overall mineralization								
EPS	–	70.03	1.67	74.05	3.84	0.0054	0.0007	0.98
Adsorption	0.05	71.47	3.73	75.93	2.92	0.0049	0.0004	0.95
	0.13	76.53	3.19	80.61	2.88	0.0045	0.0004	0.96
	0.27	67.39	3.25	71.38	2.81	0.0048	0.0005	0.95
	0.53	49.60	1.43	52.30	1.81	0.0053	0.0005	0.96
	0.80	33.04	0.37	33.06	1.00	0.0071	0.0006	0.96
	1.07	27.18	1.85	26.77	1.20	0.0062	0.0007	0.92
	1.33	20.42	1.20	21.85	1.03	0.0057	0.0007	0.93
Coprecipitation	0.01	64.09	1.76	67.90	1.80	0.0051	0.0003	0.98
	0.02	65.59	1.09	69.47	2.53	0.0041	0.0003	0.97
	0.05	57.29	1.41	61.49	2.46	0.0033	0.0003	0.97
	0.075	62.54	1.33	68.58	3.37	0.0028	0.0003	0.96
	0.10	52.22	1.23	54.67	2.17	0.0033	0.0003	0.97
	0.2	46.45	1.86	51.62	2.91	0.0028	0.0003	0.95
Mineralization of solid-bound EPS								
Adsorption	0.05	93.43	12.51	111.00	21.02	0.0020	0.0007	0.89
	0.13	65.88	8.34	79.08	18.16	0.0020	0.0008	0.84
	0.27	22.04	1.67	22.66	2.00	0.0036	0.0007	0.92
	0.53	1.25	0.31	1.48	0.10	0.0358	0.0155	0.47
	0.80	0.42	0.03	0.67	0.08	0.0468	0.0400	0.14
	1.07	0.25	0.06	0.38	0.05	0.0389	0.0326	0.07
	1.33	0.41	0.09	0.32	0.07	0.0096	0.0071	0.22
Coprecipitation	0.01	31.24	0.80	36.23	6.29	0.0022	0.0007	0.90
	0.02	18.79	0.61	21.32	3.02	0.0025	0.0007	0.92
	0.05	45.03	1.52	58.74	14.42	0.0015	0.0006	0.91
	0.075	49.66	4.77	58.75	6.92	0.0019	0.0004	0.96
	0.10	57.23	0.64	69.53	10.55	0.0017	0.0004	0.94
	0.20	53.04	2.43	65.57	16.74	0.0018	0.0008	0.86

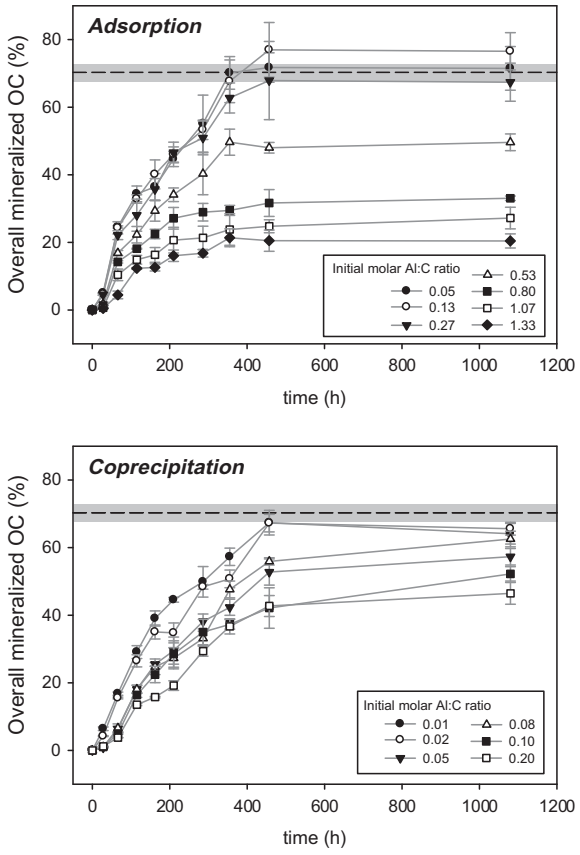

Fig. 6. Overall mineralization of EPS reacted with $Al(OH)_{3(am)}$ and $Al_{(aq)}$. The plot combines the mineralization of solid-bound EPS *and* those which did not react with $Al(OH)_{3(am)}$ or Al. The dashed line indicates the maximal average mineralization of the unreacted EPS at $t = 1100$ h. The shaded area corresponds to the respective standard error of the mean. Initial pH of the incubation suspensions was 4.5.

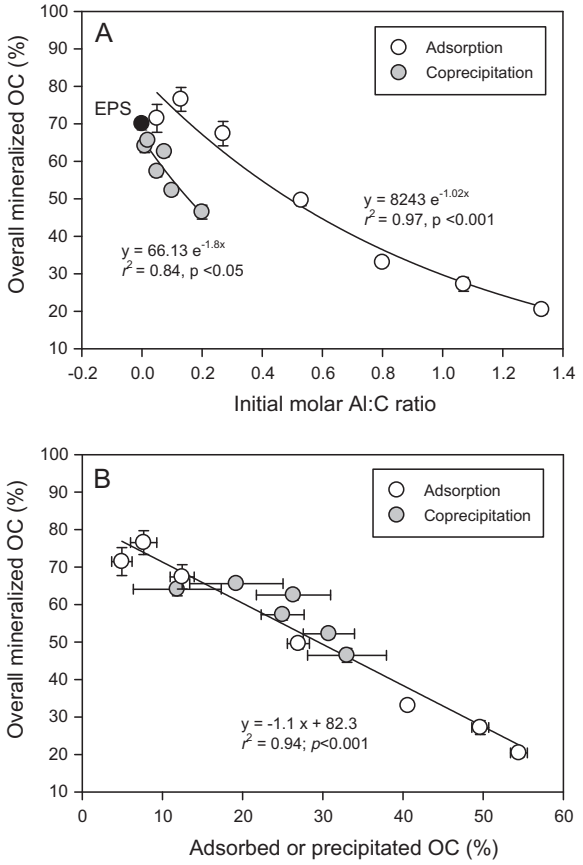

Fig. 7. (A) Overall mineralization of EPS (sum of *sorbed* and *non-sorbed* EPS following reaction) as a function of the initial molar Al:C ratio at pH 4.5. The black point reveals the mineralization of the *unreacted* EPS at a molar Al:C ratio of zero. (B) Dependence of the overall mineralization of EPS on the fractional OC adsorption and coprecipitation.

During incubation of solid-bound EPS, the pH increased by up to 2.6 units. The pH increase (0.3–2.6) was larger for those adsorption samples containing more EPS. Since the pH increase (ΔpH) for adsorption samples was positively correlated with the extent of OC desorption ($r^2 = 0.81$; $p < 0.01$; $n = 7$), we infer that desorption and subsequent protonation of EPS is likely to explain the observed pH shifts during incubation. Proton consumption by dissolution of Al phases (3 mol H^+ for 1 mol Al^{3+}) additionally contributes to the pH increase during incubation. For coprecipitates, no such pH trend was apparent; pH values increased from 4.5 to nearly constant pH 6.9 ± 0.2. Greater solid-bound EPS mineralization was observed for samples where the pH increase during incubation was larger (Fig. 11).

The two adsorption complexes examined by XPS after incubation showed that biodegradation of adsorbed EPS decreased C and N concentrations and exposed $Al(OH)_{3(am)}$ surfaces, as shown by increasing atomic Al:C ratios (Table 3). Notably, the atomic C/P ratio decreased significantly upon biodegradation, suggesting P-containing constituents being less subject to microbial utilization.

3.6. Effect of dissolved Al on biodegradation

Aqueous solutions deriving from incubation of coprecipitated EPS showed low Al concentrations (<0.11 mmol/L) whereas those from incubation of adsorption complexes had concentrations up to 1 mmol/L at the highest molar Al:C ratio. Scheel et al. (2008) observed no toxic effects of $Al_{(aq)}$ on microbial activity at concentrations up to 0.45 mmol/L at pH values of 3.8 and 4.5. Thus, we cannot fully exclude potential toxic effects on EPS mineralization for adsorption samples produced at the two largest molar Al:C ratios of 1.07 and 1.33 (which gave aqueous Al concentrations of 0.67 and 1.0 mmol/L, respectively). Aluminum toxicity is not, however, a satisfactory explanation for biodegradation trends. Given that the extent of EPS mineralization for adsorption complexes dropped rapidly with increasing molar Al:C ratio, with a large effect even for ratios much lower than those that produced significant dissolved Al (Fig. 12), we infer that EPS biodegradation was more restricted by desorption than Al toxicity. This is also supported by the clear relationship between EPS-C desorption and mineralization. Moreover, pH values at the end of incubation were >5.0 in most adsorption

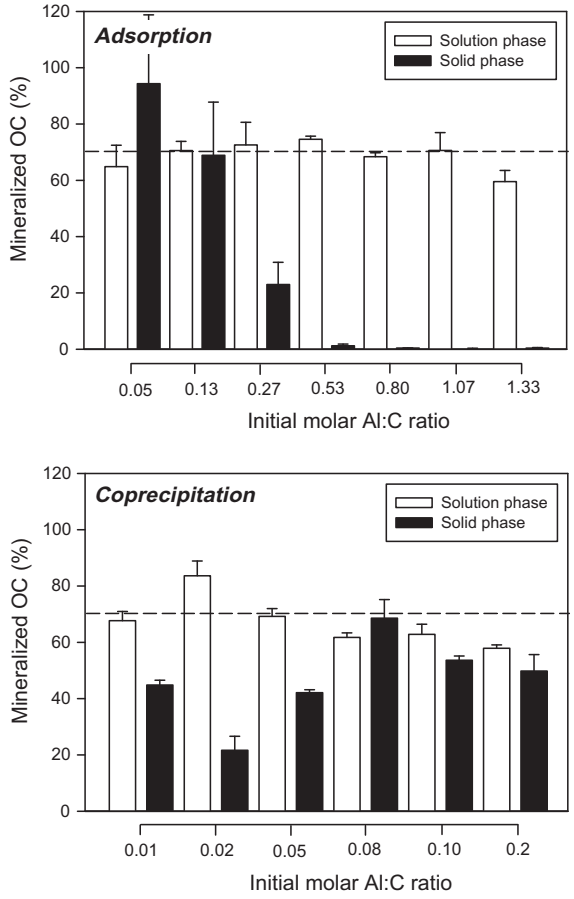

Fig. 8. Mineralization of the solid-bound EPS (black) and the non-sorbed EPS (white) following adsorption and coprecipitation. The dashed line indicates the mineralization of unreacted EPS alone (no treatment). The EPS-C concentrations (mg/g) in the adsorption complexes at the various initial Al:C ratios were 49.4 (0.05), 30.6 (0.13), 24.9 (0.27), 27.0 (0.53), 27.1 (0.80), 24.8 (1.07), and 21.8 (1.33).

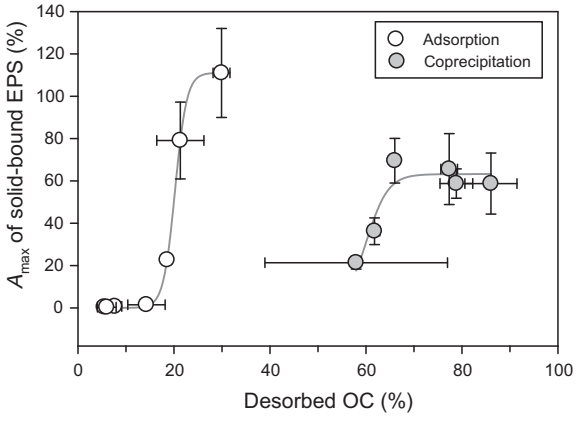

Fig. 9. Relationship between the modeled maximum mineralizable C of solid-bound EPS (A_{max}) and desorbable OC as determined in an individual desorption experiment. The initial pH in each case was 4.5.

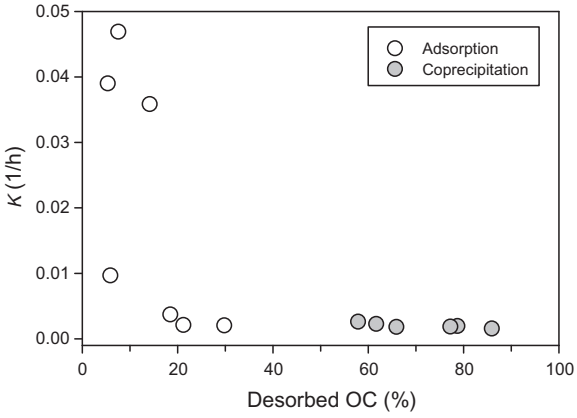

Fig. 10. Relationship between the mineralization rate constant (k) of adsorbed and coprecipitated EPS-C with desorbable OC as determined in an individual desorption experiment.

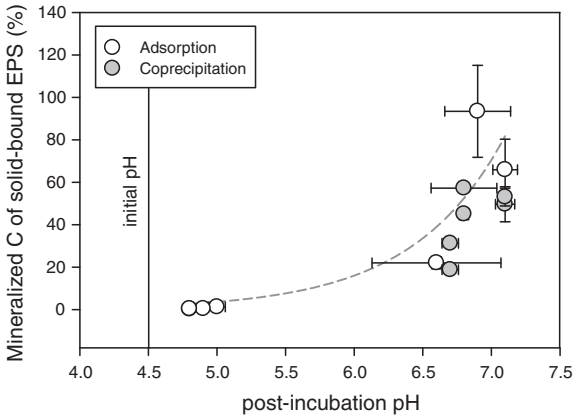

Fig. 11. Relationship between the post-incubation pH values with the observed extent of mineralization of adsorbed and coprecipitated EPS. The line serves as guide only.

treatments and, thus, only a fraction of total $Al_{(aq)}$ was present as toxic monomeric Al species.

3.7. X-ray photoelectron spectroscopy

Fig. 13 shows the XPS survey spectra of the unreacted EPS. Quantification revealed 56 atom% C, 11 atom% N, and 2 atom% P, resulting in C:N and C:P ratios of 5.2 and 26.9, respectively. Following adsorption reaction at a molar Al:C ratio of 0.53, the C:N ratio of adsorbed EPS remained similar (6.5) to that of unreacted EPS, while the C:P ratio was reduced from 27 to 15, indicating preferential adsorption of P-containing biomolecules. At larger initial molar Al:C ratio (1.33), the C:N ratio as well as the C:P ratio of adsorbed EPS approached that of unreacted EPS (Table 3). Whereas the C:N ratios of coprecipitates were again comparable to those of the unreacted EPS, the atomic C:P ratios were markedly smaller. The surface enrichment of C and N, which was calculated from the quotient of XPS- and elemental analysis-derived C and N concentrations (i.e., $C,N_{XPS}/C,N_{elemental}$), suggests potential modes

Table 3
Bulk composition and chemical environments of carbon and nitrogen in unreacted EPS and its adsorption and coprecipitation complexes as revealed by XPS.

Sample	Initial molar Al:C ratio	Treatment	O[a]	C[a]	N[a]	P[a]	Al[a]	C/N	C/P	Al/C	Surface enrichment[b]	
			atom%								C	N
$Al(OH)_{3(am)}$	–	–	63.33	6.78	BDL[c]	BDL	29.89	–	–	–	–	–
EPS	–	–	31.42	55.82	10.69	2.08	BDL	5.2	27	–	1.18	1.12
Adsorption	0.53	Pre-incubation	51.80	22.93	3.55	1.55	20.17	6.5	15	0.9	5.97	5.29
Adsorption	0.53	Post-incubation	54.63	19.04	3.04	1.87	21.41	6.3	10	1.1	9.47	ND[d]
Adsorption	1.33	Pre-incubation	51.67	23.32	3.02	0.94	21.05	7.7	25	0.9	7.43	5.18
Adsorption	1.33	Post-incubation	55.99	17.83	2.02	0.94	23.23	8.8	19	1.3	6.84	ND
Coprecipitation	0.02	–	30.24	55.38	7.70	3.46	3.22	7.2	16	0.1	1.39	1.81
Coprecipitation	0.20	–	38.34	42.43	7.18	3.69	8.35	5.9	11	0.2	2.07	2.15

Sample	Initial molar Al:C ratio	Treatment	C–(C,H)/C	C–(O,N)/C	C=O/C N–C=O/C	O–C=O/C	N–C=O/N	NH_2/N NH_3^+/N
			285.0 eV	286.6 eV	288.2 eV	289.3 eV	400.0 eV	401.7 eV
EPS	–	–	0.492	0.394	0.073	0.041	1.000	BDL
Adsorption	0.53	Pre-incubation	0.612	0.244	0.062	0.082	1.000	BDL
Adsorption	0.53	Post-incubation	0.678	0.157	0.081	0.084	1.000	BDL
Adsorption	1.33	Pre-incubation	0.698	0.196	0.049	0.057	1.000	BDL
Adsorption	1.33	Post-incubation	0.650	0.204	0.062	0.083	1.000	BDL
Coprecipitation	0.02	–	0.520	0.392	0.038	0.051	1.000	BDL
Coprecipitation	0.20	–	0.594	0.281	0.060	0.064	1.000	BDL

[a] Corrected for traces of Na and Cl.
[b] Surface enrichment = C or N (XPS)/C or N (elemental analysis).
[c] BDL, below detection limit.
[d] ND, not determined.

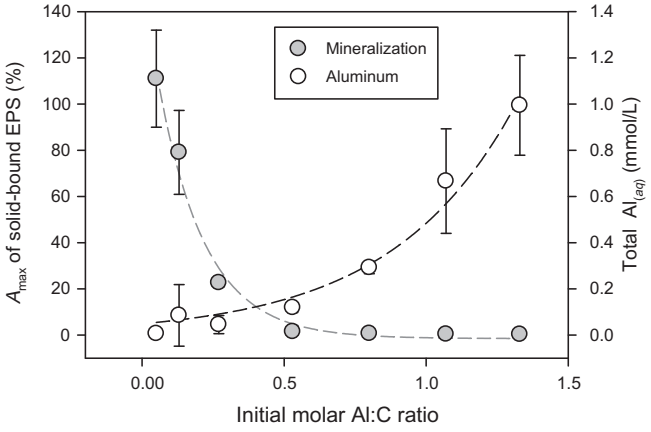

Fig. 12. Relationship of the modeled maximum mineralizable C of adsorbed EPS (A_{max}) and the total Al concentrations released during the incubations with the initial molar Al:C ratio of EPS adsorption complexes. Lines serve as guides only.

of Al–organic bonding (Mikutta et al., 2009). Enrichment factors between 5 and 7 for the adsorption complexes suggest that C and N largely accumulated at the surface of $Al(OH)_{3(am)}$ particles/aggregates. In contrast, the smaller surface C and N enrichments in coprecipitates (1.4–2.2) indicate a much more intimate mixing of the inorganic and organic phase at the nanometer depth scale probed by XPS.

The core-level carbon peak was deconvoluted into four spectral regions (Omoike and Chorover, 2004; Leone et al., 2006): (1) aliphatic C–C and C–H bondings (C–C, C–H), (2) carbon with a single bond to either oxygen or nitrogen (C–O, C–N) as in carbohydrates and amines, (3) carbon with double bonds to oxygen like in aldehydes, ketones, or amides (C=O, O=C–N), and (4) carboxylic carbon with three bondings to oxygen (O–C=O). The largest C fraction of unreacted EPS (0.492) belonged to aliphatic C as present in proteins and fatty acids followed by single bonded C–O or C–N carbons (0.394) as mainly constituting carbohydrates and proteins; carboxylic carbons only made

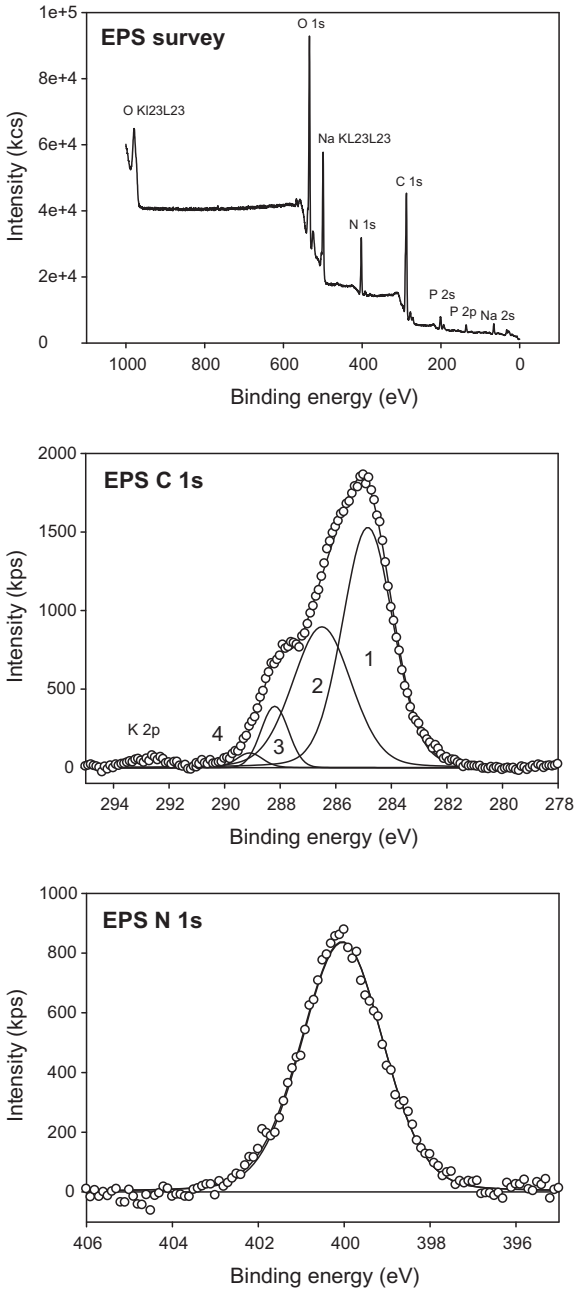

Fig. 13. Survey scan and narrow scans of C and N regions in freeze-dried EPS as detected by XPS. The C1s spectra was deconvoluted into sub-peaks according to Leone et al. (2006): (1) aliphatic C–C and C–H bondings, (2) carbon with a single bond to either oxygen or nitrogen (C–O, C–N) as found in carbohydrates and amines, (3) carbon with double bonds to oxygen as in aldehydes, ketones, or amides (C═O, O═C–N), and (4) carboxylic carbon with three bonds to oxygen (O–C═O). In contrast, the N1s peak could only be satisfactorily described by the amide N component centered at 400 eV.

a minor fraction (0.041) (Fig. 13). We reported similar proportions for *B. subtilis* EPS previously (see Table 3 in Omoike and Chorover, 2004), and comparable values have been reported for EPS extracted from mixed cultures present in activated sludge (Badireddy et al., 2010). Adsorption and coprecipitation altered the chemical composition of surface-bound EPS. Almost all treatments showed an increase (relative to unreacted EPS) in aliphatic and carboxyl C (Table 3) in the *outermost* sorbed regions that are probed by the XPS incident beam. As a result, carbon bound to oxygen or nitrogen via single bonds (C–O, C–N) decreased. The same trend was observed even when the narrow-scan C peak was charge referenced to the 285 eV signal in the survey spectrum rather than to the 400 eV N peak. This suggests that the observed fractionation pattern was independent of the correction operandi and truly represents fractionation of EPS at outer particle surfaces.

3.8. Transmission infrared spectra of non-sorbed EPS

The spectra of dissolved unreacted EPS revealed four distinct broad absorption bands assignable to (i) valence and deformation vibrations of C═O, N–H, C–N and –CO–NH– groups in the amide I ($\nu = 1654\ cm^{-1}$) and amide II region ($1544\ cm^{-1}$), (ii) symmetric stretching of C–O in carboxylate groups ($\nu_s = 1404\ cm^{-1}$), and (iii) ring vibrations of C–O–C in polysaccharides as well as symmetric stretching vibrations of P═O in the phosphodiester backbone of nucleic acids ($\nu_s = 1070\ cm^{-1}$; Table 4). Fractionation of EPS upon adsorption and coprecipitation is evident from the fact that band intensities for EPS remaining in solution were altered relative to unreacted EPS (Fig. 14). The amide I band (C═O) of protein constituents increased post-reaction for solution-phase EPS relative to the polysaccharide bands, whereas the amide II band (N–H) decreased and almost completely disappeared at high Al:C ratios. Intensities of asymmetric (present as a hump between amide I and amide II) and symmetric carboxylate (COO^-) stretching bands decreased significantly, consistent with carboxyl uptake to the Al surface. The absorption bands between ~950 and $1100\ cm^{-1}$ indicative of polysaccharides and the peak at $1235\ cm^{-1}$ corresponding to $\nu_{as}(PO_2^-)$ also decrease (e.g., in comparison to the amide I band) after both adsorption and coprecipitation. The strong absorption signal centered at $1070\ cm^{-1}$ in the polysaccharide region decreased in all samples, giving rise to relative increases in residual peaks at 1055 and $1127\ cm^{-1}$, likely reflecting ν(C–O–C) and ν(C–O–P) as in polysaccharides and phosphoesters. Noteworthy, the band at $\sim 1470\ cm^{-1}$ likely corresponding to $\delta(CH_2)$ is stronger in the spectra following coprecipitation (Fig. 14), possibly indicating that less alkyl chain components of EPS are coprecipitated with Al. The FTIR solution data suggest that $Al(OH)_{3(am)}$ and Al species have a stronger affinity for polysaccharides, carboxylate, and phosphate groups, whereas relative affinity for proteins is less clearly revealed. These trends increased with increasing initial molar Al:C ratio (Fig. 14).

3.9. DRIFT spectra of EPS adsorbed to $Al(OH)_{3(am)}$

The DRIFT spectra of adsorbed EPS are distinct from that of unreacted EPS in several regions, indicating selective uptake of particular EPS moieties. Adsorbate spectra are characterized by distinct signals in the amide I and II

Table 4
FTIR spectroscopy: band assignment in cm^{-1} according to Omoike and Chorover (2004, 2006) and references therein.

1660	νC=O of amides associated with proteins (amide I)
1544	δN–H and νC–N in –CO–NH– of proteins (amide II)
1449	$\delta_s CH_2$, and δC–OH
1403	ν_sC–O of COO^- groups
1242	ν_{as}P=O of phosphodiester backbone of nucleic acid (DNA and RNA); may also be due to phosphorylated proteins
1127	O–H deformation, νC–O, ring vibrations of polysaccharides
1078	ν_sP=O of phosphodiester backbone of nucleic acid (DNA and RNA), and phosphomonoesters (C–O–P). Also phosphorylated proteins and C–OH stretch
920	Asymmetric ester O–P–O stretching modes from nucleic acids

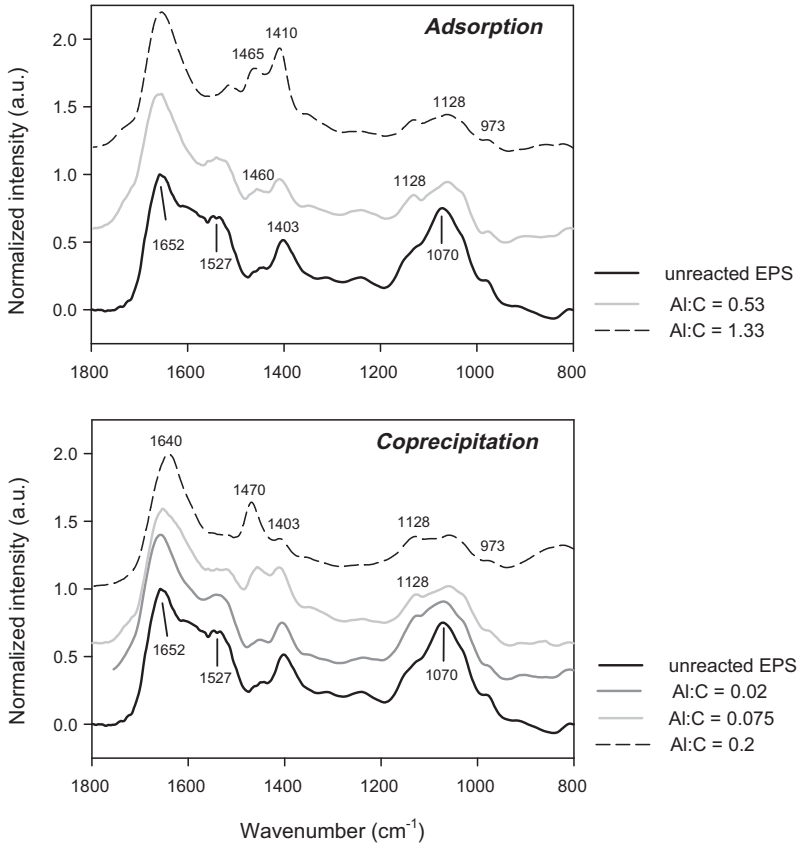

Fig. 14. Transmission IR spectra of dissolved unreacted EPS (before reaction) and non-sorbed EPS (after reaction), i.e., the fraction of EPS that remained in solution and neither adsorbed nor precipitated at the selected initial molar Al:C ratios.

region, reflecting the adsorption of protein components (Fig. 15). To quantify relative changes between unreacted and adsorbed EPS, we integrated selected spectral regions in the 800–1800 cm^{-1} range after fitting a Shirley-background and normalizing each full spectrum to unity absorbance (Unifit 8.0; Hesse et al., 2003). Integrated peak areas were obtained for the following functional units: polysaccharide/organic P (900–1200 cm^{-1}), amide I (1600–1750 cm^{-1}), amide II (1500–1600 cm^{-1}), and carboxylate groups (1385–1425 cm^{-1}). The contribution of amide II resonances declined somewhat with increasing molar Al:C ratio relative to the amide I region (Table 5). The peak maximum of the polysaccharide and phosphodiester region at 1072 cm^{-1} consistently shifted to higher frequencies upon adsorption (Fig. 15). As a result, the prominent $\nu_s(PO_2)$ peak as observed in the spectrum of unreacted EPS might be masked to some extent by this shift. While spectral resolution in the 900–1200 cm^{-1} region generally decreased (Fig. 15), the intensity in this region relative to the amide I and II peak area increased (Table 5). This indicates that polysaccharide components were selectively retained on $Al(OH)_{3(am)}$ surfaces, which agrees well with the diminished intensity of the same vibrations in transmission IR spectra of non-sorbed EPS. Symmetric stretching vibrations of carboxylate groups remained located at 1405 cm^{-1} without apparent shift in peak position. The carboxylate/(amide I + II) peak area ratio also remained about constant in adsorbed EPS (0.11–0.13).

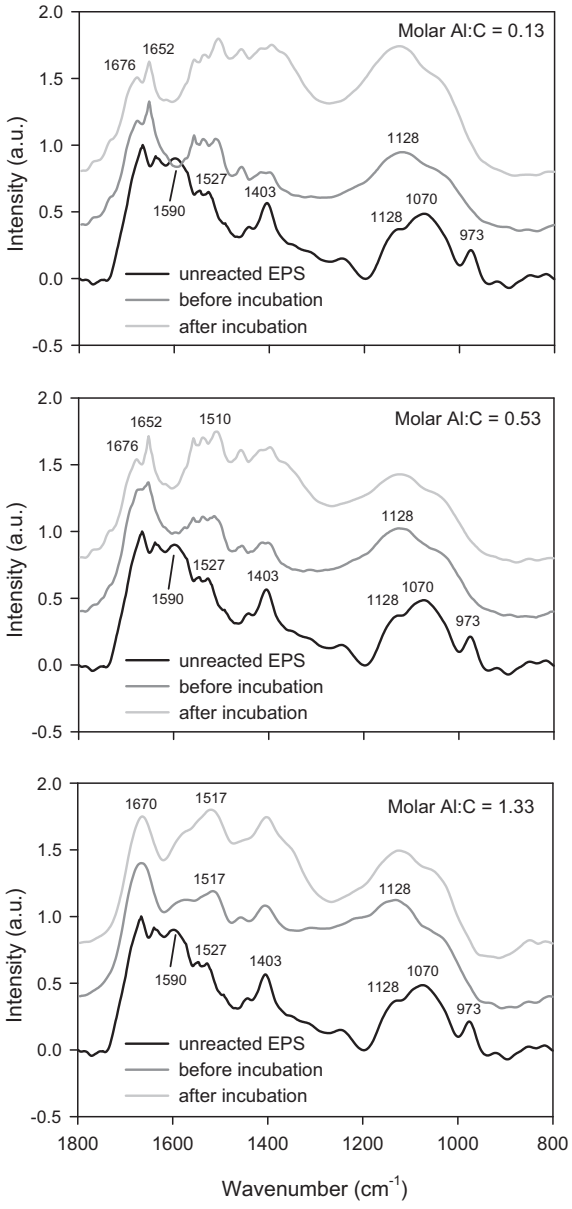

Fig. 15. DRIFT spectra of freeze-dried EPS and EPS adsorption complexes before and after incubation. Both adsorption and incubation were conducted at initial pH 4.5. The mass ratio (wt. $Al(OH)_{3(am)}$: wt. EPS) for the initial molar Al:C ratios were 2.5 (0.38), 10 (1.54), and 25 (3.85).

The DRIFT spectra of EPS following incubation were similar to those of adsorbed EPS (Fig. 15). While it is not clear to which extent fresh biomass contributes to the signals, the most apparent difference relates to a decrease of the amide I signal at $\sim$1650 cm^{-1} and a relative increase in carboxylate (1400 cm^{-1}), which is also reflected by an increasing ratio of carboxylate/(amide I + II). At the same time, the (amide I + II)/polysaccharide ratio decreased in all incubation treatments, possibly suggesting a larger stability of polysaccharides and organic P compounds compared with proteins. A larger stability of organic P compounds is also suggested by post-incubation XPS, showing smaller atomic C/P ratios when compared with the unreacted EPS (Table 3).

4. DISCUSSION

4.1. EPS adsorption versus coprecipitation

EPS represents a mixture of biomolecules, each of which contain a diversity of functional groups that influence the nature of their reactions with $Al(OH)_{3(am)}$ and dissolved Al species. In the pH range studied for EPS coprecipitation (3.8 and 4.5), soluble Al likely exists as Al^{3+} complexed with EPS with minor contributions of $AlHPO_4^+$, $AlOH^{2+}$, and $Al(OH)_2^+$ (assuming a Gaussian DOM model as substitute for EPS; Visual MINTEQ version 2.51; Gustafsson, 2006). Equilibrium calculations further suggest that at pH 3.8, $Al_{(aq)}$ concentrations are undersaturated with respect to Al solid phases at the lowest molar Al:C ratios (0.01–*ca.* 0.05), while at higher molar Al:C ratios (and at pH 4.5 for all initial Al:C ratios), $Al_{(aq)}$ concentrations were supersaturated with respect to diaspore [α-AlO(OH)], thus resulting in variable amounts of precipitated solids.

Significantly more OC was precipitated than adsorbed at comparable Al:C ratios as a result of the greater accessibility of monomeric Al species to EPS ionizable functional groups. Therefore, Al:C ratios in the coprecipitation case represent a larger fraction of EPS-reactive Al. At low pH, biomolecular charge neutralization by binding of protons and Al reduces intra- and inter-molecular coulombic repulsion, rendering EPS molecules less water-soluble and enhancing their flocculation (Tipping, 2002). In the pH range 3.5–4.5, significant flocculation and precipitation of Al- (and Fe-) natural OM complexes occur at low metal:C ratios (>0.03) (Nierop et al., 2002), and the same was observed in the current study for EPS, albeit to a different extent. Whereas Al removed >>50% of natural OM from solution at pH 4.5 and molar Al:C ratio of >0.05, (Jansen et al., 2003), only 33% of EPS-C was precipitated under comparable conditions in this study. The molecular speciation of Al is altered in such flocs, depending on incipient Al and OH^- activities, and Al:C ratio. Even at slightly acidic or neutral pH, Al speciation in flocs formed in the presence of natural OM might be limited to uncondensed monomers and small oligomers (Masion et al., 1994, 2000). Ultimately, the distribution of Al between monomeric or oligomeric OM complexes versus colloidal precipitates also depends on the relative saturation of aqueous solution with respect to precipitates that may form during the time scale of the experiment, after aqueous speciation (free monomeric versus OM-complexed Al) is accounted for.

At the smallest molar Al:C ratio (0.05), maximal surface coverage following EPS adsorption was 0.5 mg C/m^2 $Al(OH)_{3(am)}$. Similarly, synthetic goethite adsorbed maximally $\sim$13 mg EPS-C/g (I = 1 mM, pH 6) or even less at higher I, translating into a maximal surface C coverage of $\sim$0.3 mg C/m^2 (Omoike and Chorover, 2006). Fig. 16 directly compares the adsorption of EPS-C to $Al(OH)_{3(am)}$ with that of OM-C derived from less and well humified organic soil layers (Schneider et al., 2010). The data suggest that EPS from *B. subtilis* exhibit a similar sorption affinity

Table 5
Qualitative assessment of DRIFT spectra of EPS adsorbed to $Al(OH)_{3(am)}$ at various initial molar Al:C ratios after adsorption and after subsequent incubation ($n = 1$). Each functional unit was obtained from averaging 350–400 scans.

Functional unit	IR region (cm^{-1})	Unreacted EPS	Molar Al:C = 0.05		Molar Al:C = 0.53		Molar Al:C = 1.33	
				After incubation		After incubation		After incubation
Integrated peak areas (*a.u.*)								
COO^-	1385–1425	19.63	15.36	37.24	19.94	32.41	26.10	36.28
Amide I	1600–1750	94.86	81.63	78.58	92.36	79.78	94.75	86.62
Amide II	1500–1600	67.96	57.23	79.27	66.32	79.62	73.86	89.40
Amide I + II	1500–1750	162.81	138.87	157.86	158.68	159.39	168.60	176.02
Poly[a] + nucleic acids	900–1200	68.74	94.20	168.37	107.73	111.77	122.24	118.90
Functional ratios								
COO^-/amide I		0.21	0.19	0.47	0.22	0.41	0.28	0.42
COO^-/amide I + II		0.12	0.11	0.24	0.13	0.20	0.15	0.21
COO^-/Poly		0.29	0.16	0.22	0.19	0.29	0.21	0.31
Amide I/amide II		1.40	1.43	0.99	1.39	1.00	1.28	0.97
Amide I/Poly		1.38	0.87	0.47	0.86	0.71	0.78	0.73
Amide II/Poly		0.99	0.61	0.47	0.62	0.71	0.60	0.75
Amide I + II/Poly		2.37	1.47	0.94	1.47	1.43	1.38	1.48

[a] Poly, polysaccharide components.

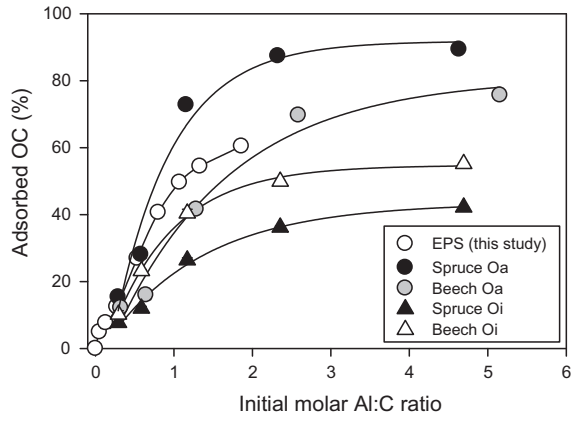

Fig. 16. Adsorption of EPS and forest floor-derived natural OM to $Al(OH)_{3(am)}$ at different initial molar Al:C ratios. Data for natural OM were taken from Schneider et al. (2010). The pH in each experiment was 4.5. Note that the initial dissolved OC concentrations (before adsorption) in the two experimental sets were different: 40 mg/L (Schneider et al., 2010) versus 100 mg/L (this study).

to $Al(OH)_{3(am)}$ as forest floor OM, even exceeding the affinity of Oa-derived OM (beech), which contains 22% aromatic C based on ^{13}C NMR (Scheel et al., 2007). Given such sorption characteristics, EPS of *B. subtilis* released into soil will readily adsorb to reactive minerals, thus conditioning mineral surfaces for microbial attachment and/or other surface reactions.

4.2. Preferential adsorption and coprecipitation of EPS components

Chemical fractionation of EPS during interaction with minerals occurs as a result of the range in functional group compositions and molecular masses of EPS components (Liu and Fang, 2002; Omoike and Chorover, 2006). Carbon and N were both adsorbed and precipitated in proportions similar to their respective prevalences in unreacted EPS, reflecting their location in similar (protein) structures. Conversely, organic P as contained in monoesters and diesters of teichoic acids, phospholipids, or nucleic acids was preferentially adsorbed and precipitated, in agreement with prior results of EPS interaction with goethite (Omoike and Chorover, 2006) and phospholipid interaction with goethite and hematite (Cagnasso et al., 2010). Interestingly, uptake of organic S compounds was non-selective during adsorption, but selective during coprecipitation. This suggests that the steric accessibility of EPS functional groups to Al plays a role in EPS fractionation. It is important to note that the nature of EPS fractionation during sorption will also vary with growth stages of microorganisms (e.g., exponential versus stationary phase) because of the associated variable contribution of major EPS components such as uronic acids, proteins, and carbohydrates (Badireddy et al., 2010).

FTIR and XP spectroscopy provide complementary molecular information about fractionation of EPS during adsorption and coprecipitation. While diffuse reflectance FTIR (DRIFT) probes bound EPS up to a sample depth of several microns, XPS data are constrained to probing the surficial 3–10 nm of the complexes due to the limited escape depth of photoelectrons. DRIFT spectroscopy indicates preferential sorption of polysaccharides and P-containing structures, while proteins were less abundant in the product solids. The partial exclusion of proteins during both adsorption and coprecipitation is also revealed by transmission FTIR of the post-reaction solution where protein band intensities increased relative to other biomolecular vibrations (Fig. 14). This result is in contrast to findings of Omoike and Chorover (2006) who observed a preferential adsorption of protein structures to goethite.

This seems to reflect a difference in reactivity between the Al and Fe bearing (oxyhydr)oxide surfaces, since the *B. subtilis* EPS employed in both studies was obtained with the same methodology. Although proteinaceous material may not have been enriched in the bulk solids, the C1s XPS results suggest that upon adsorption and coprecipitation, the contribution of aliphatic (C–C) structures as present in proteins and phospholipids increases (Table 3). We attribute this finding to the enrichment of these components in proximity to the particle surface (probed by XPS), and therefore at larger distance from the mineral–organic interface, as proteins have a weaker affinity towards direct bond formation with $Al(OH)_{3(am)}$ and Al. Moreover, bacterial remains in the outer regions of dehydrated adsorption and coprecipitation complexes may contribute to the aliphatic signal at 285 eV (Fig. 1B and C). In any case, the data indicate that the composition of freeze-dried EPS–mineral associations is heterogeneous with distance from the mineral surface. Similar findings have been obtained for mineral–organic associations in Hawaiian soils, where aromatic substances were more enriched in proximity to the contact point of mineral–organic bond formation and amide C structures increased in prevalence with distance away from the mineral–organic interface, i.e., towards the exterior surface of the complex (Mikutta et al., 2009).

4.3. Mechanisms of EPS interaction with $Al(OH)_{3(am)}$ and Al

Under the experimental conditions employed, EPS negative-charge increases with pH due to proton dissociation of carboxyl (pH 2.0–6.0), phospholipid (pH 2.4–7.2), and phosphodiester (pH 3.2–3.5) groups (Martinez et al., 2002). This gives rise to EPS electrostatic attraction to the positively charged $Al(OH)_{3(am)}$ surface (and Al species) since the point of zero charge of $Al(OH)_{3(am)}$ is between pH 7 and 9 (Hsu, 1989). In the pH range 3.8–6.5 there was no distinct pH dependence of EPS-C and EPS-N adsorption to $Al(OH)_{3(am)}$. This suggests that C- and N-containing EPS constituents (proteins, nucleic acids, polysaccharides) were proportionally removed from the solution phase. In contrast to C and N, there was a slight decline in total P (organic P and phosphate) adsorption with increasing pH, which might reflect stronger electrostatic or inner-sphere bondings of P containing constituents. The independence of EPS-C and EPS-N adsorption from pH and the slight decline in EPS-P adsorption matches the observation that pH-driven changes in adsorption of OM to variable-charge minerals frequently become apparent at pH values >6 (Geelhoed et al., 1997; Yoon et al., 2004). The contribution of strong bindings to the adsorption of poly-anionic EPS is corroborated by the missing *I* dependence for the adsorption of OC, total N, and total P, indicating that counter-ions in the background electrolyte (Na^+ and ClO_4^-) did not impair the overall adsorption process, as well as by the less pronounced EPS desorption (Fig. 9). The lack of dependence on *I* for EPS adsorption contrasts, however, with previous findings of *B. subtilis*-derived EPS adsorption to goethite (Omoike and Chorover, 2006). Similar to the aforementioned study, DRIFT spectroscopy indicates that carboxylic groups of EPS (e.g., in sugar acids or proteins) were little involved in surface complexation because adsorbed EPS showed neither an increase in the carboxylate peak at 1403 cm^{-1} nor in new peaks (1390 or 1590 cm^{-1}) assigned to metal-complexed carboxylate (Chorover and Amistadi, 2001). Given the strong adsorption of P-containing and polysaccharide components, adsorption likely is controlled by inner-sphere coordination of $Al(OH)_{3(am)}$ with phosphoryl-containing compounds such as teichoic acids, phospholipids (Cagnasso et al., 2010) or sugar acids, and weaker electrostatic interactions with less acidic polysaccharide components.

In contrast to adsorption, coprecipitation of EPS by Al revealed a significant pH and *I* dependence. More EPS (C, N, P basis) were precipitated at higher pH (4.5 versus 3.8). There are two possible explanations for this. First, at higher pH, deprotonation of phosphate and carboxyl groups allows for a more effective Al complexation and flocculation of EPS. Second, formation of secondary Al hydroxide is expected to be more intense at pH 4.5 than at pH 3.8, as confirmed by aluminum speciation calculations (Visual MINTEQ version 2.51). At pH 4.5 and the largest molar Al:C ratio (0.2), initial $Al_{(aq)}$ concentrations were supersaturated with diaspore, resulting in solid concentration of 1.6×10^{-3} mol/L versus 1.2×10^{-3} mol/L at pH 3.8. Hence, in addition to complexation with dissolved Al species, a larger fraction of EPS adsorbed to newly formed Al phases might explain the larger EPS precipitation at higher pH. Unfortunately, the small quantity of precipitated solids did not allow for further mineralogical analysis.

Adsorption of natural OM to minerals frequently increases with increasing *I* due to compression of the electric double layer (Lafrance and Mazet, 1989; Arnarson and Keil, 2000). The reverse effect was observed for EPS coprecipitation. The apparent decline in precipitated OC and total N (*ca.* −10%) and total P (*ca.* −20%) with increasing *I* suggests that counter ions (Na^+ and ClO_4^-) effectively screened the charges of EPS and Al. This reduced Al−EPS binding and consequently decreased flocculation. The screening effect is enhanced by the lower ion activity (γ coefficient) of Al^{3+} compared with Na^+ at higher *I*. The pronounced *I*-dependence of coprecipitation, overall, suggests that weaker coulombic (cation/anion exchange and hydrogen bondings) or non-coulombic forces (van der Waals) contribute much more to EPS coprecipitation than to EPS adsorption. As a consequence, coprecipitated EPS was also more easily mobilized than adsorbed EPS in the desorption treatment (Fig. 5). The fact that no further difference was observed in OC, N, and P coprecipitation at larger *I* (170 versus 1700 mM) could result from contraction of the EPS at higher *I* (Omoike and Chorover, 2006), thus minimizing the number of functional groups per molecule involved in EPS–Al interaction.

4.4. Stability of adsorbed and coprecipitated EPS

Bacterial EPS, an intrinsically labile C source, was significantly stabilized against microbial decay by both adsorption to $Al(OH)_{3(am)}$ and coprecipitation with Al. Summation of the mineralized fractions of *solid*-phase and *non-sorbed* products of Al–EPS interaction indicates

that both adsorption and coprecipitation result in an overall stabilization, i.e., the total biodegradation was diminished relative to unreacted EPS. The same has been observed for forest floor leachates (Oi, Oa) adsorbed to $Al(OH)_{3(am)}$ (Schneider et al., 2010). This effect is limited by reactive Al; at small Al:C ratios, stabilization of sorbed OM is less pronounced. Increased C bioavailability with decreasing molar Al:C ratio was also observed by Boudot et al. (1989) for synthetic metal–organic complexes (citrate, fulvic and humic acid-like materials) during a 44-day incubation experiment (pH 5.4–5.6). The larger EPS biodegradation in coprecipitates formed at low molar Al:C ratios (<0.05) may additionally be caused by the larger contribution of labile Al−EPS complexes when compared with coprecipitates formed at higher molar ratios.

In the case of adsorbed EPS, no net stabilization was observed at initial Al:C ratios <0.53, corresponding to an EPS-C content of >~30 mg/g $Al(OH)_{3(am)}$ or EPS loadings of >0.3 mg/m^2. For forest floor leachates, we recently observed that for low suspension concentrations of $Al(OH)_{3(am)}$, co-adsorbed phosphate blocked sorption sites for DOM molecules, thereby resulting in weaker mineral–organic bonding and enhanced mineralization (Schneider et al., 2010). Fig. 17 demonstrates that for the EPS adsorption complexes, the concentration of co-adsorbed phosphate also increased with decreasing $Al(OH)_{3(am)}$ availability up to ~3.5 μmol/m^2. Assuming complete surface coverage of Al (hydr)oxide by phosphate to occur at 3.5–4.5 μmol/m^2 (Borggaard et al., 2005), most sorption sites were occupied by phosphate at Al:C <0.5. In addition to blocking reactive surface aluminol groups, where EPS functionalities could otherwise form inner-sphere complexes via ligand exchange, phosphate adsorption also diminishes long-range electrostatic attraction for EPS by decreasing $Al(OH)_{3(am)}$ surface charge. Thus, competitive phosphate adsorption gives rise to weaker mineral–organic bonding overall. At larger molar Al:C ratios with less competition by phosphate, strong attachment of EPS to $Al(OH)_{3(am)}$ reduced desorption and rendered EPS less bioavailable.

EPS detachment from Al-bearing solids was enhanced by the weaker EPS–Al bonding that occurred with increased surface OC loading. Fewer ligand–metal bonds and increased repulsive forces of solid-bound EPS (partly by co-adsorbed phosphate) both favor EPS detachment (Kaiser and Guggenberger, 2007) and thus biodegradation (Mikutta et al., 2007). The pronounced EPS sorption–desorption hysteresis also suggests that strong chemical bonds render adsorbed EPS less prone to desorption while weaker bonds in coprecipitates foster EPS mobilization and mineralization. The observed correlation between desorption and mineralization (e.g., Fig. 9) supports the view that free EPS serve as the principal energy and C source for microbial decomposers. This is in agreement with mineralization studies utilizing DOM and different minerals including goethite, vermiculite, and pyrophyllite (Mikutta et al., 2007) and $Al(OH)_{3(am)}$ (Schneider et al., 2010). In line with the latter study, we also found that smaller Al:C ratios with weaker mineral–organic bonding resulted in the largest increase in pH during incubation, the greatest fractional release of EPS and, hence, greater mineralization. In contrast, larger Al availability favors stronger bonds, less variation in incubation pH, and thus, on average, less desorption and mineralization (Fig. 11).

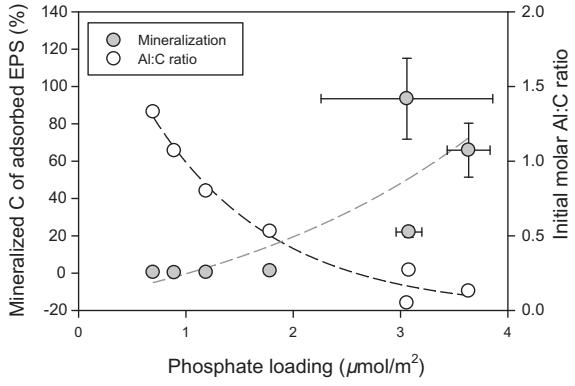

Fig. 17. Relationship between the loading of co-adsorbed phosphate and (i) the extent of mineralization of adsorbed EPS (A_{1100h}) and (ii) the initial molar Al:C ratio.

4.5. Extent of stabilization: EPS versus forest-floor OM

Although mineralization rates from different studies cannot be quantitatively compared without ambiguity, qualitative comparison provides a means to account for the effectiveness of mineral surfaces in stabilization of EPS and other OM types. In our comparison (Fig. 18), we rely on adsorption complexes of $Al(OH)_{3(am)}$ with forest floor-derived OM, being representative for temperate forest ecosystems and spanning a wide range in chemical properties and biological stabilities (Schneider et al., 2010). For example, the OM from an Oa horizon under spruce that was rich in aromatic C (31%) exhibited low mineralization (~10%; Schneider et al., 2010). In contrast, the corresponding Oi horizon being relatively depleted in aromatic C (7%),

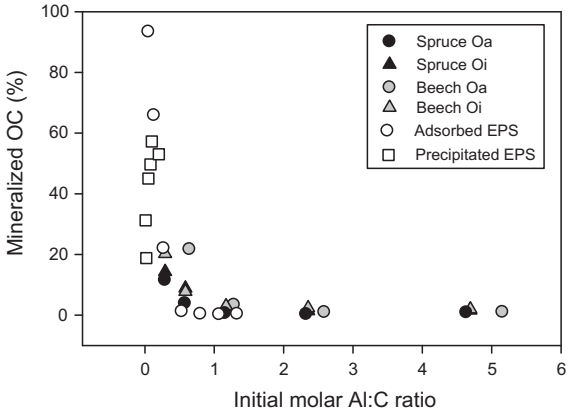

Fig. 18. Comparison of the extent of mineralization of EPS in complexes produced by adsorption and coprecipitation (this study) with those of forest floor-derived OM adsorbed to $Al(OH)_{3(am)}$ (Schneider et al., 2010). Note that the initial dissolved OC concentrations (before adsorption) in the two experimental sets were different: 40 mg/L (Schneider et al., 2010) versus 100 mg/L (this study).

was more mineralizable (~46%). The respective adsorption complexes with $Al(OH)_{3(am)}$ were incubated under comparable conditions as used in this study (initial pH 4.5; same inoculum as in the EPS treatment).

Comparison of data sets from the two studies indicates that the extent of EPS mineralization was consistent with those of more structurally diverse forest floor OM types at initial Al:C ratios of >0.1 (Fig. 18). In both cases, at smaller initial molar Al:C ratios, OC mineralization was increased due to enhanced competition effects (phosphate) and electrostatic repulsive forces. This result clearly highlights the fact that, irrespective of OM source and inherent recalcitrance (e.g., based on aromatic C content), mineral surfaces can effectively decelerate microbial decomposition if sufficient bonding sites are available and competition effects (e.g., with phosphate) are minimal. Moreover, mineralization *rates* of adsorbed and coprecipitated EPS are similar to those of lignin-derived, aromatic DOM leached from an Oa horizon that has been subsequently adsorbed to goethite, pyrophyllite, and vermiculite (Fig. 19). This is surprising given that pyrophyllite and vermiculite lack significant permanent charge (pyrophyllite) or singly-coordinated OH groups (pyrophyllite, vermiculite) and thus are considered less reactive towards OM. Given comparable mineralization of adsorbed EPS and OM from organic soil layers at larger initial molar Al:C ratio (0.53), we conclude that adsorption processes stabilize microbial EPS as efficiently as is the case for plant-derived OM. This is an intriguing result since effective attachment of EPS to minerals would initially imply a costly energy investment by source microorganisms. However, such investment is reasonable if a principal EPS function is, in fact, to condition mineral surfaces for adhesion, biofilm formation, or the acquisition of (mineral-hosted) nutrients.

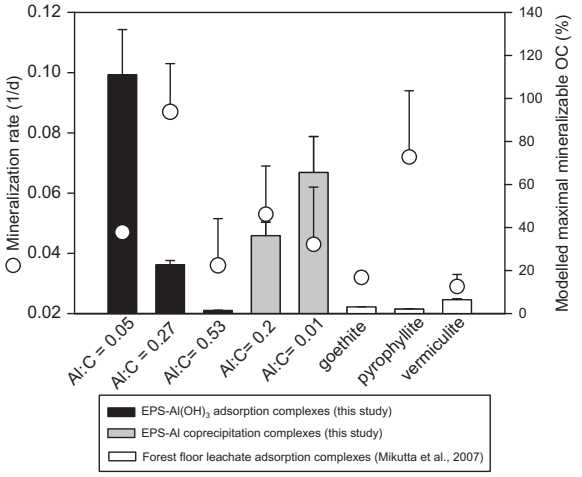

Fig. 19. Comparison of the mineralization rates (left *y*-axis) and the extent of mineralization of EPS complexes (right *y*-axis) produced by adsorption and coprecipitation (this study) with those of forest-floor OM adsorbed to goethite, pyrophyllite, and vermiculite at pH 4.0 (Mikutta et al., 2007). The latter data have been obtained using the published mineralization curves, which have been re-fitted with the one-pool degradation model (Eq. (6)) in order to facilitate comparison. Goodness of fits was reflected by r^2 values of 0.88–1.00.

5. IMPLICATIONS

Bacterial EPS fulfill important functions in soil environments such as attaching bacteria to mineral surfaces, protecting them from dehydration, or capturing nutrients. Once exuded from the cell, a portion of EPS can be adsorbed to minerals or flocculated by Al, thus being temporarily removed from the biological cycle. During both adsorption and coprecipitation reactions, EPS become fractionated with respect to structural components. Organic phosphorus compounds, like teichoic or nucleic acids, preferentially react with $Al(OH)_{3(am)}$ and Al while no such selectivity was observed for organic C and organic N. Hence, EPS might represent an important source of stable organic P in soils. Inner-sphere coordination of phosphoryl groups is a likely contributing factor. Overall weaker binding in coprecipitates results in enhanced mobilization and, thus, microbial utilization of precipitated versus adsorbed EPS (except at very low Al:C ratios). The availability of sorption sites, operationalized as initial molar Al:C ratio, was the master variable controlling the stability of solid-bound EPS. The stability of EPS can vary dramatically from very low, as observed for dissolved EPS to extremely high, for the case where reactive minerals are present in sufficient quantity. Therefore, the effect of EPS–mineral interaction on C stabilization cannot, at present, be reliably assessed *a priori* when the availability of sorption sites in soil is unknown. More generally, a greater importance of such stabilized microbial products can be expected in subsoil horizons where competition effects are minor (less C coverage) and where elevated pH values favor precipitation of aqueous Al (and Fe). The observed functional dependence between EPS desorption and biodegradation confirms trends previously observed in other mineral–(natural) OM systems. This study also demonstrates that precipitation of EPS by dissolved Al can lead to significant EPS immobilization. Although being intrinsically labile, strongly-bound EPS resists biodegradation and, thus, might contribute to long-term C sequestration in soils.

ACKNOWLEDGMENTS

We are grateful to the members of the Central Analytical Department of BayCEER for their support and Mary Kay Amistadi for collecting the FTIR data. Axel Schippers is acknowledged for analysis of microbial residues in EPS. Financial support was provided by the German Research Foundation. J.D.C. gratefully acknowledges support of NSF Grant DEB-0543130. We also gratefully acknowledge the comments of three anonymous reviewers and Susan Glasauer.

REFERENCES

Aguilera A., Souza-Egipsy V., Martin-Uriz P. S. and Amils R. (2008) Extraction of extracellular polymeric substances from extreme acidic microbial biofilms. *Curr. Adv. Appl. Microbiol. Biotechnol.* **78**, 34–66.

Arnarson T. S. and Keil R. G. (2000) Mechanisms of pore water organic matter adsorption to montmorillonite. *Mar. Chem.* **71**, 309–320.

Badireddy A. R., Chellam S., Gassman P. L., Engelhard M. H., Lea A. S. and Rosso K. M. (2010) Role of extracellular polymeric substances in bioflocculation of activated sludge microorganisms under glucose-controlled conditions. *Water Res.* **44**, 4505–4516.

Badireddy A. R., Korpol B. R., Chellam S., Gassman P. L., Engelhard M. H., Lea A. S. and Rosso K. M. (2008) Spectroscopic characterization of extracellular polymeric substances from *Escherichia coli* and *Serratia marcescens*: suppression using sub-inhibitory concentrations of bismuth thiols. *Biomacromolecules* **9**, 3079–3089.

Bartels H. and Wrbitzky R. (1959) Bunsenscher Absorptionskoeffizient des Kohlendioxyds in Wasser und Plasma zwischen 15 und 38 °C. *Naturwissenschaften* **46**, 667.

Beveridge T. J., Makin S. A., Kadurugamuwa J. L. and Li Z. (1997) Interactions between biofilms and the environment. *FEMS Microbiol. Rev.* **20**, 291–303.

Borggaard O. K., Raben-Lange B., Gimsing A. L. and Strobel B. W. (2005) Influence of humic substances on phosphate adsorption by aluminum and iron oxides. *Geoderma* **127**, 270–279.

Boudot J.-P., Bel Hadj Brahim A., Steiman R. and Seigle-Murandi F. (1989) Biodegradation of synthetic organo-metallic complexes of iron and aluminum with selected metal to carbon ratios. *Soil Biol. Biochem.* **21**, 961–966.

Cagnasso M., Boero V., Franchini M. A. and Chorover J. (2010) ATR-FTIR studies on phospholipid vesicle interactions with α-FeOOH and α-Fe_2O_3 surfaces. *Colloids Surf. B* **76**, 456–467.

Chorover J. and Amistadi M. K. (2001) Reaction of forest floor organic matter at goethite, birnessite and smectite surfaces. *Geochim. Cosmochim. Acta* **65**, 95–109.

Davis J. A. (1982) Adsorption of natural dissolved organic matter at the oxide/water interface. *Geochim. Cosmochim. Acta* **46**, 2381–2393.

de Brouwer J. F. C., Wolfstein K. and Stal L. J. (2002) Physical characterization and diel dynamics of different fractions of extracellular polysaccharides in an axenic culture of a benthic diatom. *Eur. J. Phycol.* **37**, 37–44.

Ding Y.-X., Chin W.-C., Rodriguez A., Hung C.-C., Santschi P. H. and Verdugo P. (2008) Amphiphilic exopolymers from *Sagittula stellata* induce DOM self-assembly and formation of marine microgels. *Mar. Chem.* **112**, 11–19.

Dufrêne Y. F., van der Wal A., Norde W. and Rouxhet P. G. (1997) X-ray photoelectron spectroscopy analysis of whole cells and isolated cell walls of gram-positive bacteria: comparison with biochemical analysis. *J. Bacteriol.* **179**, 1023–1028.

Esparza-Soto M. and Westerhoff P. (2003) Biosorption of humic and fulvic acids to live activated sludge biomass. *Water Res.* **37**, 2301–2310.

Geelhoed J. S., Hiemstra T. and Van Riemsdijk W. H. (1997) Phosphate and sulfate adsorption on goethite: single anion adsorption and competitive adsorption. *Geochim. Cosmochim. Acta* **61**, 2389–2396.

Guibaud G., van Hullebusch E. and Bordas F. (2006) Lead and cadmium biosorption by extracellular polymeric substances (EPS) extracted from activated sludges: pH-sorption edge tests and mathematical equilibrium modeling. *Chemosphere* **64**, 1955–1962.

Gustafsson J. P. (2006) *Visual Minteq 2.40. KTH*. Department of Land and Water Resources Engineering, Stockholm, Sweden.

Hesse R., Chassé T. and Szargan R. (2003) Unifit 2002 – universal analysis software for photoelectron spectra. *Anal. Bioanal. Chem.* **375**, 856–863.

Hsu P. H. (1989) Aluminum oxides and oxyhydroxides. In *Minerals in Soil Environments*, second ed. (eds. J. B. Dixon and S. B. Weed). SSSA Book Series Nr. 1, Madison, WI, pp. 331–371.

Jaisi D. B., Dong H., Kim J., He Z. and Morton J. P. (2007) Nontronite particle aggregation induced by microbial Fe(III) reduction and exopolysaccharide production. *Clays Clay Miner.* **55**, 96–107.

Jansen B., Nierop K. G. J. and Verstraten J. M. (2003) Mobility of Fe(II), Fe(III) and Al in acidic forest soils mediated by dissolved organic matter: influence of solution pH and metal/organic carbon ratios. *Geoderma* **113**, 323–340.

Kaiser K. and Guggenberger G. (2000) The role of DOM sorption to mineral surfaces in the preservation of organic matter in soils. *Org. Geochem.* **31**, 711–725.

Kaiser K. and Guggenberger G. (2007) Sorptive stabilization of organic matter by microporous goethite: sorption into small pores vs. surface complexation. *Eur. J. Soil Sci.* **58**, 45–59.

Kiran B. and Kaushik A. (2008) Chromium binding capacity of *Lyngbya putealis* exopolysaccharides. *Biochem. Eng. J.* **38**, 47–54.

Kumar A. S., Mody K. and Jha B. (2007) Bacterial exopolysaccharides: a perception. *J. Basic Microbiol.* **47**, 103–117.

Lafrance P. and Mazet M. (1989) Adsorption of humics substances in the presence of sodium salts. *J. Am. Water Works Assoc.* **81**, 155–162.

Leone L., Loring J., Sjöberg S., Persson P. and Shchukarev A. (2006) Surface characterization of the Gram-positive bacteria *Bacillus subtilis* – an XPS study. *Surf. Interface Anal.* **38**, 202–205.

Liu H. and Fang H. H. P. (2002) Characterizing the electrostatic binding sites of extracellular polymers by linear programming analysis of titration data. *Biotechnol. Bioeng.* **80**, 806–811.

Makarov M. I., Haumaier L., Zech W., Marfenina O. E. and Lysak L. V. (2005) Can ^{31}P NMR spectroscopy be used to indicate the origins of soil organic phosphates? *Soil Biol. Biochem.* **37**, 15–25.

Marschner B., Brodowski S., Dreves A., Gleixner G., Gude A., Grootes P. M., Hamer U., Heim A., Jandl G., Ji R., Kaiser K., Kalbitz K., Kramer C., Leinweber P., Rethemeyer J., Schäffer A., Schmidt M. W. I., Schwark L. and Wiesenberg G. L. B. (2008) How relevant is recalcitrance for the stabilization of organic matter in soils? *J. Plant Nutr. Soil Sci.* **171**, 91–110.

Martinez R. E., Smith D. S., Kulczycki E. and Ferris F. G. (2002) Determination of intrinsic bacterial surface acidity constants using a Donnan shell model and a continuous pK_a distribution method. *J. Colloid Interface Sci.* **253**, 130–139.

Masion A., Bottero J.-Y., Thomas F. and Tchoubar D. (1994) Chemistry and structure of Al(OH)/organic precipitates. A small-angle X-ray scattering study. 2. Speciation and structure of the aggregates. *Langmuir* **10**, 4349–4352.

Masion A., Vilge-Ritter A., Rose J., Stone W. E. E., Teppen B. J., Rybacki D. and Bottero J.-Y. (2000) Coagulation–flocculation of natural organic matter with Al salts: speciation and structure of the aggregates. *Environ. Sci. Technol.* **34**, 3242–3246.

Mikutta R., Mikutta C., Kalbitz K., Scheel T., Kaiser K. and Jahn R. (2007) Biodegradation of forest floor organic matter bound to minerals via different binding mechanisms. *Geochim. Cosmochim. Acta* **71**, 2569–2590.

Mikutta R., Schaumann G., Gildemeister D., Bonneville S., Kramer M. G., Chorover J., Chadwick O. A. and Guggenberger G. (2009) Biogeochemistry of mineral–organic associations across a long-term mineralogical soil gradient (0.3–4100 kyr), Hawaiian Islands. *Geochim. Cosmochim. Acta* **73**, 2034–2060.

Mikutta R., Chadwick O. A., Chorover J., Dörr N., Kaiser K., Kramer M. G., Vollmer A. and Guggenberger G. (2010) Mineralogical impact on organic nitrogen across a long-term

soil chronosequence (0.3–4100 kyr). *Geochim. Cosmochim. Acta* **74**, 2142–2164.

Nierop K. G. J., Jansen B. and Verstraten J. M. (2002) Dissolved organic matter, aluminum and iron interactions: precipitation induced by metal/carbon ratio, pH and competition. *Sci. Total Environ.* **300**, 201–211.

Omoike A. and Chorover J. (2004) Spectroscopic study of extracellular polymeric substances from *Bacillus subtilis*: aqueous chemistry and adsorption effects. *Biomacromolecules* **5**, 1219–1230.

Omoike A., Chorover J., Kwon K. D. and Kubicki J. D. (2004) Adhesion of bacterial exopolymers to α-FeOOH: inner-sphere complexation of phosphodiester groups. *Langmuir* **20**, 11108–11114.

Omoike A. and Chorover J. (2006) Adsorption to goethite of extracellular polymeric substances from *Bacillus subtilis*. *Geochim. Cosmochim. Acta* **70**, 827–838.

Paul E. A. and Clark F. E. (1996) *Soil Microbiology and Biochemistry*. Academic Press, San Diego.

Scheel T., Jansen B., van Wijk A. J., Verstraten J. M. and Kalbitz K. (2008) Stabilization of dissolved organic matter by aluminum: a toxic effect or stabilization through precipitation? *Eur. J. Soil Sci.* **59**, 1122–1132.

Scheel T., Dörfler C. and Kalbitz K. (2007) Precipitation of dissolved organic matter by aluminum stabilizes carbon in acidic forest soils. *Soil Sci. Soc. Am. J.* **71**, 64–74.

Schneider M. P. W., Scheel T., Mikutta R., van Hees P. and Kalbitz K. (2010) Sorptive stabilization of organic matter by amorphous Al hydroxide. *Geochim. Cosmochim. Acta* **74**, 1606–1619.

Tipping E. (2002) *Cation Binding by Humic Substances. Cambridge Environmental Chemistry Series No. 12*. Cambridge University Press, Cambridge.

Watanabe M., Suzuki Y., Sasaki K., Nakashimada Y. and Nishio N. (1999) Flocculating property of extracellular polymeric substance derived from a marine photosynthetic bacterium, *Rhodovulum* sp. *J. Biosci. Bioeng.* **87**, 625–629.

Whitman W. B., Coleman D. C. and Wiebe W. J. (1998) Prokaryotes: the unseen majority. *Proc. Natl. Acad. Sci. USA* **95**, 6578–6583.

Yoon T. H., Johnson S. B. and Brown, Jr., G. E. (2004) Adsorption of Suwannee River fulvic acid on aluminum oxyhydroxide surfaces: an in situ ATR-FTIR study. *Langmuir* **20**, 5655–5658.

Zhu J., Yang P., Li B., Zhang J. and Huang Q. (2008) Microcalorimetric studies of interaction between extracellular polymeric substance and sulfide minerals. *Trans. Nonferrous Met. Soc. China* **18**, 1439–1442.

Associate editor: Susan Glasauer